ENGINEERING OF BIOMATERIALS

INŻYNIERIA BIOMATERIAŁÓW

JOURNAL OF POLISH SOCIETY FOR BIOMATERIALS AND FACULTY OF MATERIALS SCIENCE AND CERAMICS / AGH UNIVERSITY

CZASOPISMO POLSKIEGO STOWARZYSZENIA BIOMATERIAŁÓW I WYDZIAŁU INŻYNIERII MATERIAŁOWEJ I CERAMIKI / AGH

Number 171
Numer 171
Volume XXVI
Rocznik XXVI

Year 2023
(Issue 4)
Rok 2023
(Zeszyt 4)

ISSN 1429-7248

PUBLISHER:
WYDAWCA:

Polish Society for Biomaterials in Krakow
Polskie Stowarzyszenie Biomateriałów w Krakowie

EDITORIAL COMMITTEE:
KOMITET REDAKCYJNY:

Editor-in-Chief
Redaktor naczelny
Elżbieta Pamuła

Editor
Redaktor
Patrycja Domalik-Pyzik

Secretary of editorial
Sekretarz redakcji
Design
Projekt
Katarzyna Trała

ADDRESS OF EDITORIAL OFFICE:
ADRES REDAKCJI:

AGH University of Krakow
30/A3, Mickiewicz Av.
30-059 Krakow, Poland
Akademia Górniczo-Hutnicza
al. Mickiewicza 30/A-3
30-059 Kraków

Issue: 250 copies
Nakład: 250 egz.

Scientific Publishing House AKAPIT
Wydawnictwo Naukowe AKAPIT
e-mail: wn@akapit.krakow.pl

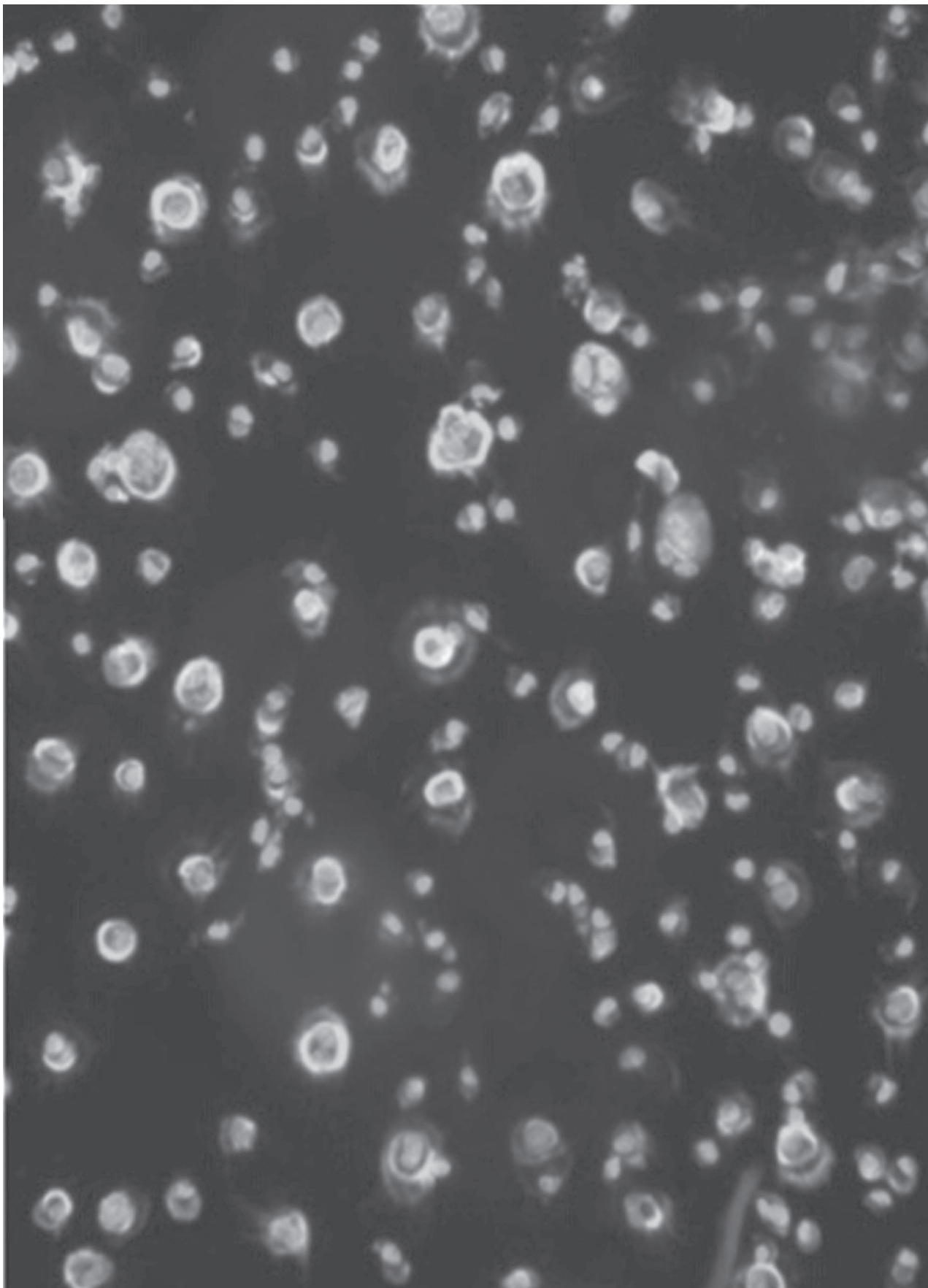

ENGINEERING OF BIOMATERIALS

EDITORIAL BOARD
KOMITET REDAKCYJNY

INTERNATIONAL EDITORIAL BOARD
MIĘDZYNARODOWY KOMITET REDAKCYJNY

ENGINEERING OF BIOMATERIALS

Wskazówki dla autorów

1. Prace do opublikowania w kwartalniku „Engineering of Biomaterials / Inżynieria Biomateriałów" przyjmowane będą wyłącznie w języku angielskim.
2. Wszystkie nadsyłane artykuły są recenzowane.
3. Materiały do druku prosimy przysyłać za pomocą systemu online (www.biomaterials.pl).
4. Struktura artykułu:
• TYTUŁ • Autorzy i instytucje • Streszczenie (200-250 słów) • Słowa kluczowe (4-6) • Wprowadzenie • Materiały i metody • Wyniki i dyskusja • Wnioski • Podziękowania • Piśmiennictwo
5. Autorzy przesyłają pełną wersję artykułu, łącznie z ilustracjami, tabelami, podpisami i literaturą w jednym pliku. Artykuł w tej formie przesyłany jest do recenzentów. Dodatkowo autorzy proszeni są o przesłanie materiałów ilustracyjnych (rysunki, schematy, fotografie, wykresy) w oddzielnych plikach (format np. .jpg, .gif., .tiff, .bmp). Rozdzielczość rysunków min. 300 dpi. Wszystkie rysunki i wykresy powinny być czarno-białe lub w odcieniach szarości i ponumerowane cyframi arabskimi. W tekście należy umieścić odnośniki do rysunków i tabel.
6. Na końcu artykułu należy podać wykaz piśmiennictwa w kolejności cytowania w tekście i kolejno ponumerowany.
7. Redakcja zastrzega sobie prawo wprowadzenia do opracowań autorskich zmian terminologicznych, poprawek redakcyjnych, stylistycznych, w celu dostosowania artykułu do norm przyjętych w naszym czasopiśmie. Zmiany i uzupełnienia merytoryczne będą dokonywane w uzgodnieniu z autorem.
8. Opinia lub uwagi recenzentów będą przekazywane Autorowi do ustosunkowania się. Nie dostarczenie poprawionego artykułu w terminie oznacza rezygnację Autora z publikacji pracy w naszym czasopiśmie.
9. Za publikację artykułów redakcja nie płaci honorarium autorskiego.
10. Adres redakcji:

Czasopismo
„Engineering of Biomaterials / Inżynieria Biomateriałów"
Akademia Górniczo-Hutnicza im. St. Staszica
Wydział Inżynierii Materiałowej i Ceramiki
al. Mickiewicza 30/A-3, 30-059 Kraków
tel. (48) 12 617 44 48, 12 617 25 61
e-mail: epamula@agh.edu.pl, kabe@agh.edu.pl

Szczegółowe informacje dotyczące przygotowania manuskryptu oraz procedury recenzowania dostępne są na stronie internetowej czasopisma:
www.biomaterials.pl

Instructions for authors

1. Papers for publication in quarterly journal „Engineering of Biomaterials / Inżynieria Biomateriałów" should be written in English.
2. All articles are reviewed.
3. Manuscripts should be submitted to editorial office through online submission system (www.biomaterials.pl).
4. A manuscript should be organized in the following order:
• TITLE • Authors and affiliations • Abstract (200-250 words) • Keywords (4-6) • Introduction • Materials and Methods • Results and Discussion • Conclusions • Acknowledgements • References
5. All illustrations, figures, tables, graphs etc. preferably in black and white or grey scale should be additionally sent as separate electronic files (format .jpg, .gif., .tiff, .bmp). High-resolution figures are required for publication, at least 300 dpi. All figures must be numbered in the order in which they appear in the paper and captioned below. They should be referenced in the text. The captions of all figures should be submitted on a separate sheet.
6. References should be listed at the end of the article. Number the references consecutively in the order in which they are first mentioned in the text.
7. The Editors reserve the right to improve manuscripts on grammar and style and to modify the manuscripts to fit in with the style of the journal. If extensive alterations are required, the manuscript will be returned to the authors for revision.
8. Opinion or notes of reviewers will be transferred to the author. If the corrected article will not be supplied on time, it means that the author has resigned from publication of work in our journal.
9. Editorial does not pay author honorarium for publication of article.
10. Address of editorial office:

Journal
„Engineering of Biomaterials / Inżynieria Biomateriałów"
AGH University of Krakow
Faculty of Materials Science and Ceramics
30/A-3, Mickiewicz Av., 30-059 Krakow, Poland
tel. (48) 12) 617 44 48, 12 617 25 61
e-mail: epamula@agh.edu.pl, kabe@agh.edu.pl

Detailed information concerning manuscript preparation and review process are available at the journal's website:
www.biomaterials.pl

STUDIA PODYPLOMOWE
Biomateriały – Materiały dla Medycyny
2023/2024

Organizator: Akademia Górniczo-Hutnicza im. Stanisława Staszica w Krakowie Wydział Inżynierii Materiałowej i Ceramiki Katedra Biomateriałów i Kompozytów **Kierownik:** prof. dr hab. inż. Elżbieta Pamuła **Sekretarz:** dr inż. Katarzyna Reczyńska-Kolman	**Adres:** 30-059 Kraków, Al. Mickiewicza 30 Pawilon A3, p. 208 lub p. 210 tel. 12 617 44 48, 12 617 23 38 email: epamula@agh.edu.pl; kmr@agh.edu.pl https://www.podyplomowe.agh.edu.pl/studia-podyplomowe-kursy-doksztalcajace-i-szkolenia/biomaterialy-materialy-dla-medycyny/
Charakterystyka: Tematyka prezentowana w trakcie zajęć obejmuje przegląd wszystkich grup materiałów dla zastosowań medycznych: metalicznych, ceramicznych, polimerowych, węglowych i kompozytowych. Słuchacze zapoznają się z metodami projektowania i wytwarzania biomateriałów a następnie możliwościami analizy ich właściwości mechanicznych, właściwości fizykochemicznych (laboratoria z metod badań: elektronowa mikroskopia skaningowa, mikroskopia sił atomowych, spektroskopia w podczerwieni, badania energii powierzchniowej i zwilżalności) i właściwości biologicznych (badania: *in vitro* i *in vivo*). Omawiane są regulacje prawne i aspekty etyczne związane z badaniami na zwierzętach i badaniami klinicznymi (norma EU ISO 10993). Słuchacze zapoznają się z najnowszymi osiągnięciami w zakresie nowoczesnych nośników leków, medycyny regeneracyjnej i inżynierii tkankowej.	
Sylwetka absolwenta: Studia adresowane są do absolwentów uczelni technicznych (inżynieria materiałowa, technologia chemiczna), przyrodniczych (chemia, biologia, biotechnologia) a także medycznych, stomatologicznych, farmaceutycznych i weterynaryjnych, pragnących zdobyć, poszerzyć i ugruntować wiedzę z zakresu inżynierii biomateriałów i nowoczesnych materiałów dla medycyny. Słuchacze zdobywają i/lub pogłębiają wiedzę z zakresu inżynierii biomateriałów. Po zakończeniu studiów wykazują się znajomością budowy, właściwości i sposobu otrzymywania materiałów przeznaczonych dla medycyny. Potrafią analizować wyniki badań i przekładać je na zachowanie się biomateriału w warunkach żywego organizmu. Ponadto słuchacze wprowadzani są w zagadnienia dotyczące wymagań normowych, etycznych i prawnych niezbędnych do wprowadzenia nowego materiału na rynek. Ukończenie studiów pozwala na nabycie umiejętności przygotowywania wniosków do Komisji Etycznych i doboru metod badawczych w zakresie analizy biozgodności materiałów.	
Zasady naboru: Termin zgłoszeń: od 20.09.2023 do 20.10.2023 (liczba miejsc ograniczona - decyduje kolejność zgłoszeń) Wymagane dokumenty: dyplom ukończenia szkoły wyższej Osoby przyjmujące zgłoszenia: prof. dr hab. inż. Elżbieta Pamuła (pawilon A3, p. 208, tel. 12 617 44 48, e-mail: epamula@agh.edu.pl) dr inż. Katarzyna Reczyńska-Kolman (pawilon A3, p. 210, tel. 12 617 23 38, e-mail: kmr@agh.edu.pl)	
Czas trwania: 2 semestry (od XI 2023 r. do VI 2024 r.) 8 zjazdów (soboty-niedziele) 1 raz w miesiącu przewidywana liczba godzin: 160	**Opłaty:** 3 000 zł (za dwa semestry)

33rd Biomaterials in Medicine and Veterinary Medicine

Annual Conference

10 – 13 October 2024 Rytro, Poland

SAVE THE DATE

10-13

OCTOBER

2024

www.biomat.agh.edu.pl

REGISTER

AND

SUBMIT

AN ABSTRACT

SPIS TREŚCI
CONTENTS

Wersja papierowa czasopisma „Engineering of Biomaterials / Inżynieria Biomateriałów" jest jego wersją pierwotną
Printed version of „Engineering of Biomaterials / Inżynieria Biomateriałów" is a primary version of the journal

LIPID MICROPARTICLES AS QUERCETIN CARRIERS FOR THE TREATMENT OF BURN WOUNDS: MANUFACTURING, PROPERTIES, AND *IN VITRO* STUDIES ON MACROPHAGES POLARIZATION

Julia Stępień[1]*, Anna Kusibab[1], Ana Beatriz Sousa[2,3], Judite Novais Barbosa[2,3], Elżbieta Pamuła[1]

[1] AGH University of Krakow,
Faculty of Materials Science and Ceramics,
Department of Biomaterials and Composites,
al. A. Mickiewicza 30, 30-059 Krakow, Poland
[2] Instituto de Investigação e Inovação em Saúde da Universidade do Porto,
Rua Alfredo Allen, 208, 4200-125 Porto, Portugal
[3] ICBAS - Instituto de Ciências Biomédicas Abel Salazar, Universidade do Porto,
R. Jorge de Viterbo Ferreira 228,
4050-313 Porto, Portugal
*e-mail: stepienjulia98@gmail.com

Abstract

Burn wounds are a unique type of injury that can affect the entire body and cause irreversible damage. They are characterized by significant morbidity and mortality due to the pathophysiology of the healing process manifested by unremitting inflammation, leading to a critical need to search for new treatments. This study focuses on the development of drug delivery systems in the form of lipid microparticles loaded with quercetin, as an agent to combat acute inflammation in burn wounds. We aimed to explore the effect of quercetin in modulating macrophage polarization from proinflammatory (M1) to anti-inflammatory (M2) phenotype. The absence of a cytotoxic effect of the produced particles on macrophages, as well as the lack of negative effects on their morphology was proven. The study confirmed the ability of quercetin and quercetin-loaded lipid microparticles to modulate macrophage polarization in an anti-inflammatory direction, based on the analysis of their surface markers expression performed with the use of flow cytometry. With the use of quercetin, the expression of M2 specific marker increased. Furthermore, better results were obtained for encapsulated quercetin, confirming the necessity of encapsulation to increase the therapeutic potential.

***Keywords**: lauric acid, quercetin, encapsulation, cytotoxicity, macrophage polarization, burn wounds*

[Engineering of Biomaterials 171 (2023) 2-11]

doi:10.34821/eng.biomat.171.2023.2-11

Submitted: 2023-09-18, Accepted: 2023-10-19, Published: 2023-10-23

Introduction

Wound healing is a complex process regulated chemically, by molecules such as growth factors or cytokines, and mechanically, by tension of the skin or cell contraction forces. This process consists of overlapping phases, namely homeostasis, inflammation, proliferation, maturation, and remodeling [1].

The inflammatory phase (4-6 days) involves clot formation, platelet activation, and neutrophil and monocyte-driven debris removal. Macrophages are known to clean the wound site and release growth factors and cytokines inducing inflammation. During the proliferation phase (up to 3 weeks), the most important phenomena is related to granulation tissue formation, deposition of extracellular matrix (ECM), angiogenesis, and epithelialization. Guided by growth factors and ECM proteins, fibroblasts and endothelial cells proliferate, to cover the wound site and achieve wound closure. In the maturation and remodeling phase (from day 8 to ~1 year) collagen is reorganized and ECM is remodeled by metalloproteinases. Collagen type III is replaced with collagen type I, angiogenesis stabilizes, and the scar matures, resulting in a lower strength of the healed tissue. Cellular and molecular interactions drive wound closure and tissue repair [1-6].

In the burn wound healing process, these three phases can also be distinguished; however, in this type of injuries, recovery is more complicated, it takes longer to move from one phase to the next, and the inflammatory response is stronger. Burn wounds can be classified according to their total body surface area (TBSA) into major and minor (>10% of TBSA) wounds [7-11]. In addition, it is also important to classify the injury according to its depth and size. Skin burn injuries can be classified as partial or full thickness. If the injury affects the upper layer of the skin (only the epidermis), it is classified as a superficial burn (first-degree). Superficial partial thickness (second-degree) burns involve the epidermis and part of the dermis. In superficial and superficial partial-thickness burns, most of the adnexal structures (hair follicles, sweat, and sebaceous glands) are preserved. Deep partial-thickness (second-degree) burns destroy a larger proportion of the dermis, some adnexal structures, and partially pain receptors. A full-thickness burn (third-degree) destroys the whole epidermis, dermis, and all adnexal structures. It is not typically painful due to damage of the nerve endings. Fourth-degree burns involve damage of deeper tissues, such as muscle or bone, and often lead to loss of the burden part [7].

In the case of extensive burn injuries, there is an unprecedented inflammatory response, which distinguishes this type of harm from other traumas. The cellular defense mechanisms begin with the proinflammatory phase, known as the systemic inflammatory response syndrome. Macrophages produce proinflammatory mediators and biochemical cytokines, such as tumor necrosis factor alpha (TNF-α) and interleukin-6 (IL-6). Thermal injury results in prolonged and profound hypermetabolism, which leads to an increased production of proinflammatory cytokines, as well as the formation of reactive oxygen species (ROS). Free radicals are known to have a beneficial effect on antimicrobial action and wound healing; however, in the case of burns, they are produced in enormous amounts, leading to infection and sepsis, tissue damage, and multiple organ failure [7,10-12].

This response of the body makes it very important to fight inflammation in an early stage of treatment. This applies mainly to superficial partial thickness burns, which do not require surgical intervention, and when treating them, the most important step is covering the wound at the early stage. Topical antimicrobials are fundamental to non-surgical approaches. These dressings are applied to cover burn wounds, promote epithelialization, prevent infection and mechanical trauma, keeping wounds moist and reducing pain. The ideal dressing for burn wounds should also have the ability to fight inflammation and do not require frequent changes, which is especially painful in the case of burns. However, none of the dressings currently clinically used possess all of these features. Drug delivery systems are expected to be beneficial for the treatment of this type of burn wounds, due to their ability to meet all or most of the requirements for ideal burn wound dressings [7,10,11,13].

One of the compounds that show the potential to reduce inflammation is quercetin. Quercetin is a plant-derived flavonoid that can be found in fruits (e.g., apples, grapes, berries), vegetables (e.g., capers, brassica vegetables, onions, tomatoes), and in herbs and medical plants (e.g., tea, elderberry). It has many desirable properties to be explored in medicine, such as various bactericidal mechanisms and biofilm destruction ability. Furthermore, it is recognized to have antioxidant and anti-inflammatory properties. Quercetin is known to scavenge free radicals and interact with cellular molecules influencing their antioxidant activity. Supporting cellular antioxidant capacity is mainly based on upregulating the expression of specific molecules, for example, glutathione (GSH), which are able to neutralize free radicals and transfer their harmful effects to less sensitive cell structures (e.g., from the lipid membrane to the cytosol). Direct actions include, for example, antilipoperoxidative activity and hydrogen donating ability [14-18].

The main goal of this study was to develop a drug delivery system in the form of lipid microparticles loaded with quercetin and to evaluate their potential to influence the polarization of human macrophages towards a M2 anti-inflammatory phenotype. The use of macrophages for *in vitro* studies is related to their crucial role in modulating inflammation in the body. The microparticles, manufactured by a hot emulsification method, were evaluated in terms of the morphology, size, and encapsulation efficiency of quercetin. *In vitro* studies focused on evaluating the cytotoxic effect of microparticles on human macrophages, the influence of quercetin on cell morphology, and the ability of the particles to modulate macrophage polarization toward an anti-inflammatory phenotype.

Materials and Methods

Manufacturing of quercetin carriers

Lauric acid (MKBR440v – SIGMA-ALDRICH) was chosen as a lipid matrix for the production of particles. The hot emulsification method was used to produce microparticles (microparticle production scheme shown in FIG. 1). The water phase was a solution of 10% poly(vinyl alcohol) (Mowiol® 4-88 – SIGMA ALDRICH), and the oil phase was lauric acid – for the unloaded microparticles, or lauric acid and quercetin (QE) (Q4951-10G – SIGMA-ALDRICH) – for the loaded microparticles. Briefly, the oil phase was melted in a water bath at 65°C. After homogenization, the oil phase was combined with the water phase, then the mixture was poured into liquid nitrogen and left to thaw. Microparticles were manufactured with different QE concentrations: 5%, 10%, and 20% (w/w).

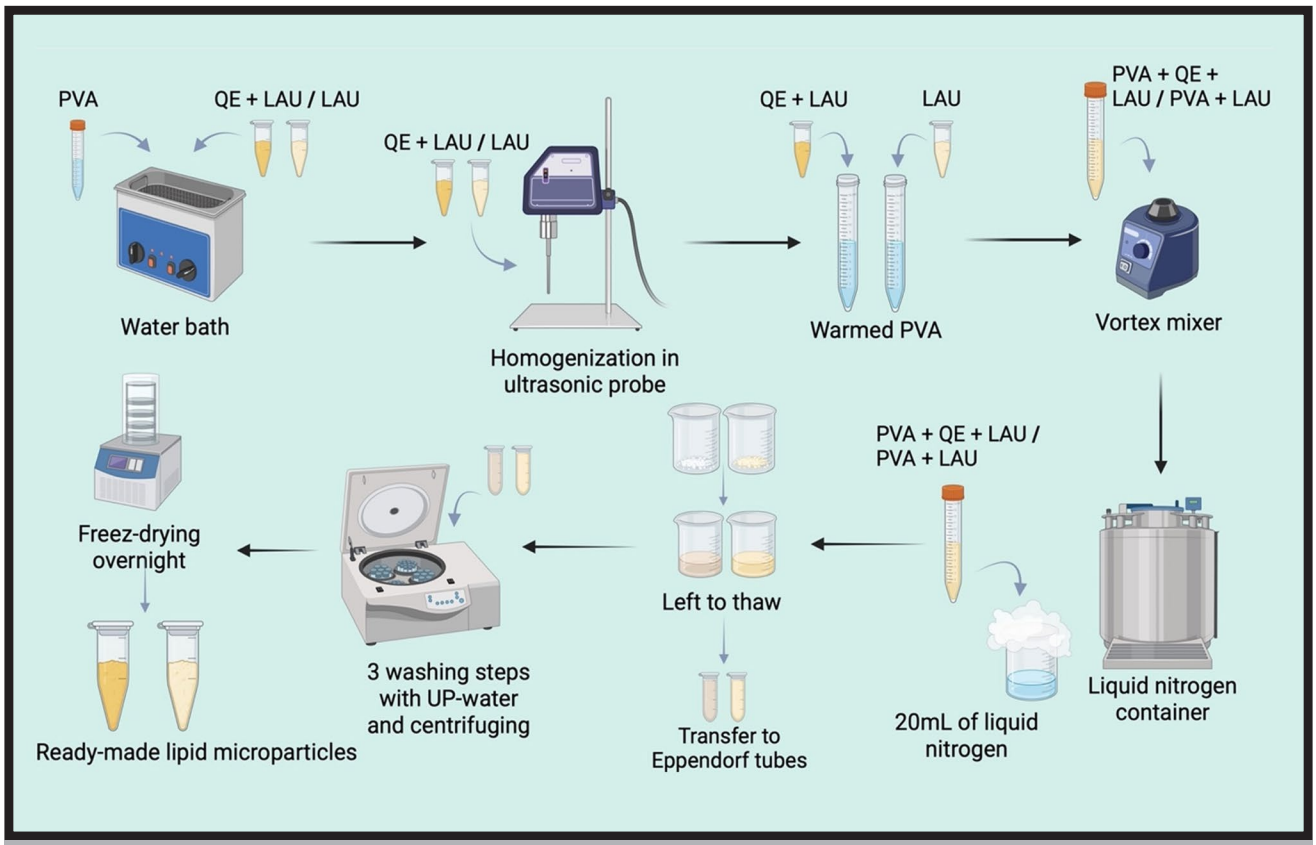

FIG. 1. Scheme of production of lipid microparticles by the hot emulsification method.

Particles size and morphology

In order to evaluate particles morphology, pictures were taken under an optical microscope (ZEISS, Axiovert 40 CFL). On their basis, the shape and size of the particles were assessed. The particle size distribution was also evaluated using the program ImageJ.

Fourier-transform infrared spectroscopy (FTIR)

FTIR was used to confirm the presence of QE in the lipid microparticles. Before FTIR examination, the samples were placed in a vacuum oven, at room temperature, for 2 days for thorough drying. The particles and QE powder were then mixed in a mortar with KBr in a 2:200 ratio. In the case of the QE powder, less quantity was used, due to its intensive color.

Before testing the samples, background measurement was made (without a sample) to calibrate the device. Then the samples were sequentially placed in the FTIR device (PerkinElmer) for measurements with the same parameters for all the samples (initial energy: 5624, resolution 4 cm^{-1}, OPD: 0.2, detector: MIR TGS and scan range at: 4000-400 cm^{-1}).

Monocytes isolation and differentiation into macrophages

To evaluate the anti-inflammatory potential of the QE loaded particles, primary human macrophages were selected for *in vitro* tests, due to their significant contribution to maintaining inflammation in burn wounds. Human monocytes were isolated from the peripheral blood of healthy donors, by negative selection, using the RosetteSep Monocyte Enrichment antibody cocktail (STEMCELL Technologies, Inc.). The samples were obtained from the Centro Hospitalar Universitário de São João (CHUSJ) in Porto. The use of human blood samples for research was approved by the CHUSJ Ethics Committee for Health (references 90/19 and 260/11). All procedures were performed in agreement with the Helsinki Declaration and the Oviedo Convention and all donors gave their written consent before blood collection.

Briefly, after buffy coats were centrifuged, peripheral blood mononuclear cells (PBMC) were separated, treated with a cocktail of specific antibodies, and diluted with a fetal bovine serum (FBS) solution. This mixture was then layered over a density gradient medium, Histopaque-1077, and centrifuged to isolate monocytes. Monocytes were washed, counted and cultured on coverslips in a 24-well plate.

For macrophage differentiation, $0.5 \cdot 10^6$ monocytes/mL were seeded on glass coverslips in 24-well plates (500 µL/well) and cultured for 7 days. Monocytes were cultured in complete Roswell Park Memorial Institute (RPMI) 1640 media (Corning) containing L-glutamine and supplemented with 10% FBS (Sigma-Aldrich). After 7 days, cell culture medium was replaced.

To activate monocytes toward an M1-like phenotype, monocytes/macrophages were stimulated with 10 ng/mL lipopolysaccharide (LPS derived from *Escherichia coli* O55:B5, Sigma-Aldrich Co., St Louis, MO, USA) and 50 ng/mL interferon gamma (IFN-γ, ImmunoTools, Friesoythe, Germany). The experimental protocol is shown in FIG. 2.

The developed microparticles and pure quercetin (resuspended in cell culture medium) were added to the culture on day 8 and left in contact with the cells for 24 h. The following samples were studied: unloaded particles at a concentration of 0.15 mg/ml, quercetin-loaded particles at 0.15 mg/ml concentration (theoretical quercetin content 0.0075 mg/ml), quercetin-loaded particles at 0.30 mg/ml concentration (theoretical quercetin content 0.015 mg/ml) and pure quercetin at a concentration of 0.15 mg/ml. Production efficiency was calculated from the formula:

$$P_f = \frac{m_f}{m_i} \cdot 100\%$$

where:
m_i – initial mass of ingredients,
m_f – final mass of the obtained microparticles.

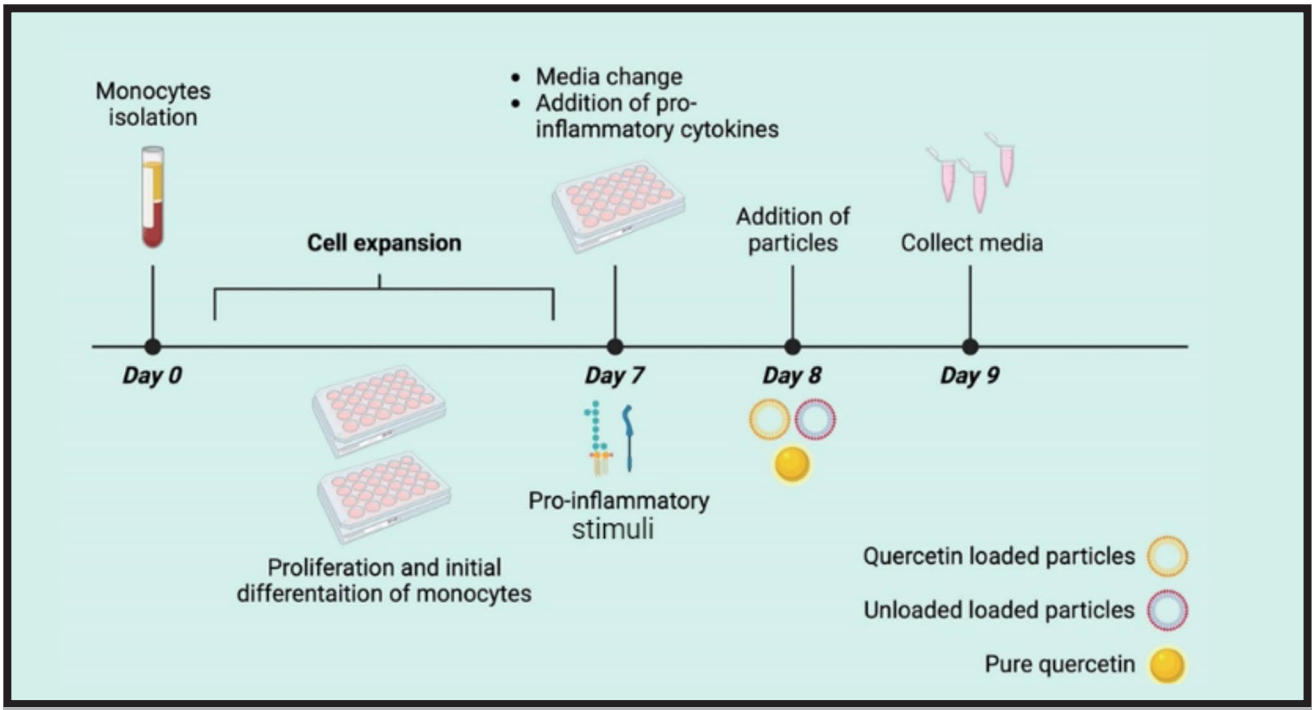

FIG. 2. Experimental design used for the establishment of proinflammatory conditions. Cells were left to differentiate for 7 days. On day 7, proinflammatory stimuli (LPS and IFN-γ) were added to the culture. On day 8, manufactured particles were added, and on day 9 the cells were fixed and the cell culture media was collected for further analysis.

Cytotoxicity test

The cytotoxic effect of the particles on macrophages was evaluated by measuring lactate dehydrogenase (LDH) levels, which is an enzyme present inside cells. During the death of a cell, LDH escapes into the medium, and by measuring its level, it is possible to determine the number of cells that have died. On this basis, the cytotoxicity of the material is determined. The LDH assay was performed according to the manufacturer's protocol (CytoTox 96® Non-Radioactive Cytotoxicity Assay, Promega Corporation, Madison, WI, USA). Briefly, 50 µL of culture medium was added to 50 µL of Substrate Mix. Following a 30 min incubation at room temperature, the reaction was stopped with 50 µL of the Stop Solution. The optical density of the plate was read with a microplate reader (Synergy Mx, BioTek, Vernusky, VT, USA) set at 490 nm. The cytotoxicity threshold was calculated by dividing the negative control (100% live cells) by the positive control (100% dead cells) multiplied by 100%. The value obtained determines the number above which the molecules show cytotoxicity. Positive control was obtained with the use of lysis buffer provided by the manufacturer.

Influence of quercetin on macrophages morphology

Nuclei and actin staining were performed to assess macrophage morphology. Phalloidin red (diluted in a ratio of 1:200, A12381; ThermoFisher Scientific, Invitrogen) and 4′,6-diamidino-2-phenylindole (DAPI diluted in a ratio of 1:1000, D3571; Alfagene) were used for staining.

Influence of quercetin on macrophages polarization

To evaluate the influence of quercetin encapsulated in microparticles and of pure quercetin on macrophages polarization, flow cytometry assays were performed. Human CD14 antibody (21279146; ImmunoTools) was used as a pan macrophage marker. Cells after 48 h of incubation with microparticles or pure quercetin were stained with antibody and examined with a flow cytometer (BD FACSCanto IITM flow cytometer, Becton Dickinson). For antibody staining, cells were transferred to a 96-well plate. Staining solutions were prepared separately for each condition, by combining 2 µL of CD14 antibody and completed with FACS buffer to achieve a final volume of 50 µL. Cells were incubated with staining solutions for 30 min and then cleaned with FACS buffer.

Results

Evaluation of particles morphology

Microparticles were characterized based on microscopic images (FIG. 3) and their size was measured in the ImageJ program (FIG. 4). The microparticles have a round, regular shape, and those loaded with quercetin had a yellow-greenish color. The coloration of the particles may be due to the presence of quercetin inside. It can be observed that particles do not have a tendency to aggregate; they exist as individual entities. Aggregation occurs only in particular locations and can be caused by a large number of particles in the sample.

According to the size distribution histograms of all analyzed samples, microparticles with a size lower than 2 µm predominate (FIG. 3). Unloaded (FIG. 3A) and 5% QE samples (FIG. 3B) consist of microparticles up to 12 µm in size, while for 10% QE (FIG. 3C) and 20% QE samples (FIG. 3d) microparticles with a size up to 18 µm were present. The median particle size for all samples varied between 1.52 µm and 2.16 µm.

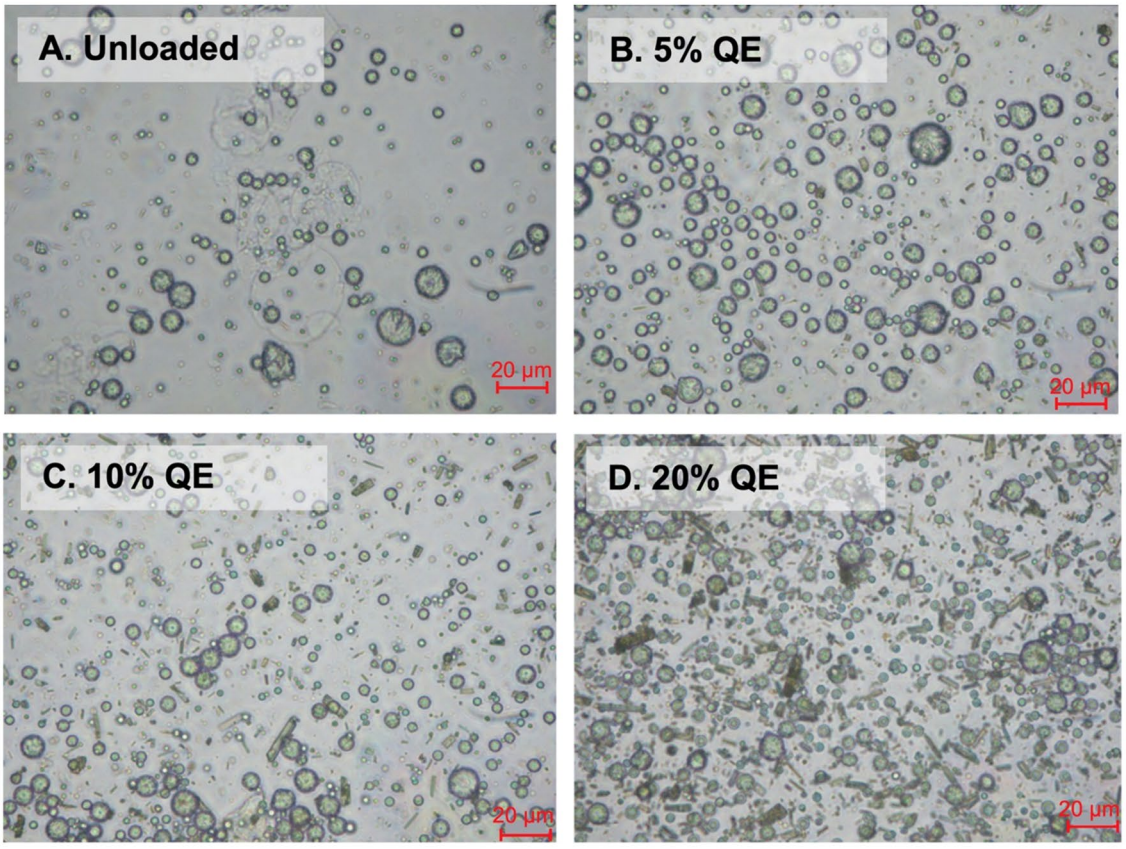

FIG. 3. Microscopic image of manufactured particles: A. unloaded, B. loaded with 5% QE, C. loaded with 10% QE, and D. loaded with 20% QE; scale bar = 20 µm.

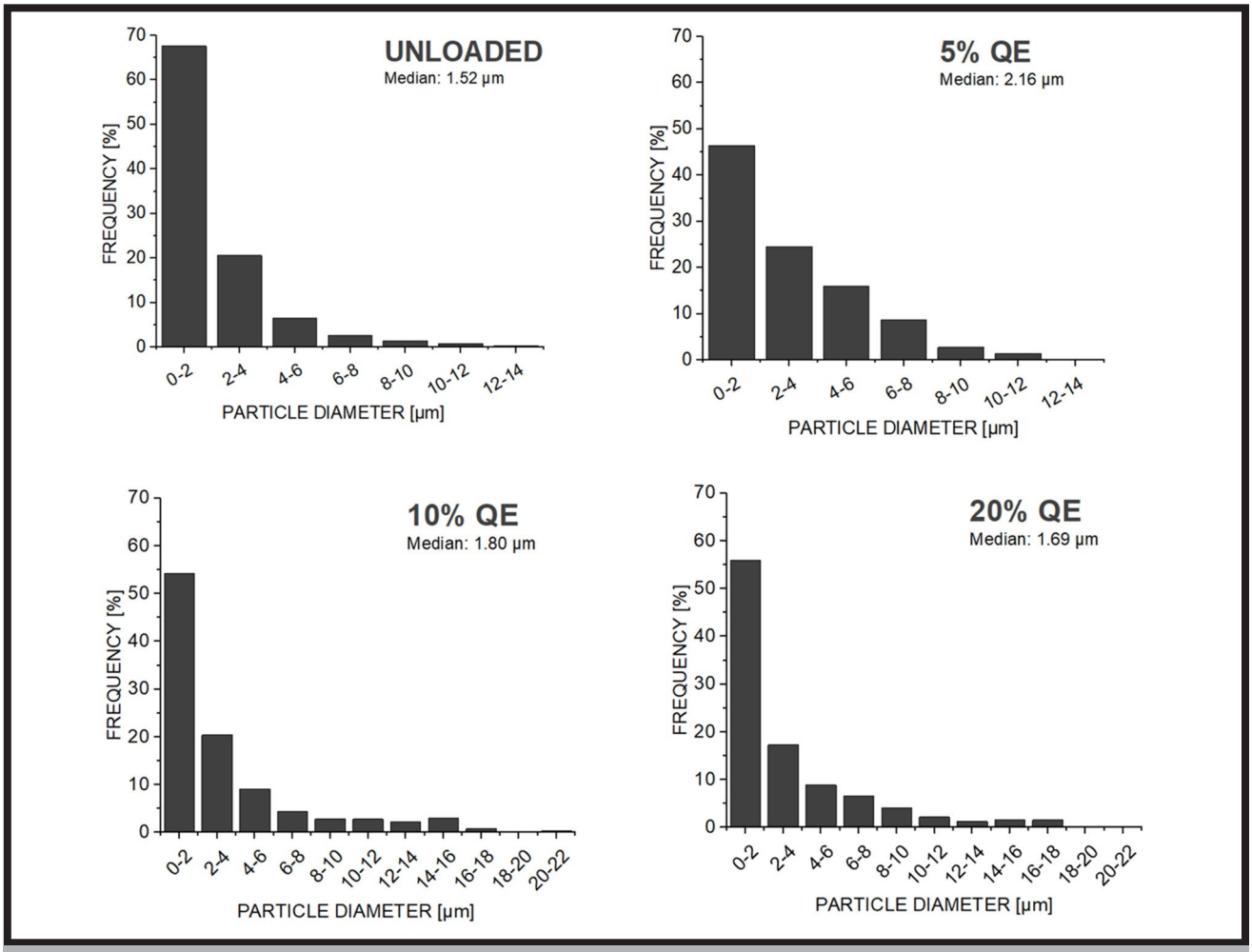

FIG. 4. Size distribution of manufactured particles: A. unloaded, B. loaded with 5% QE, C. loaded with 10% QE, and D. loaded with 20% QE. $\tilde{x}_n$ = 384 of measured particles per condition.

Fourier-transform infrared spectroscopy (FTIR)

For FTIR analysis, characteristic bonds in quercetin were found: hydroxyl group (–OH) and carbonyl group (C=O) bonds were selected for analysis (marked in FIG. 5A). The analysis of lauric acid involved peaks originating from the carboxyl group (–COOH) and a methylene group ($–CH_2$), which were chosen for analysis (as marked in FIG. 5B).

The bonds were marked on the spectra shown in FIG. 6 with letters: A – OH stretching vibrations in quercetin, B – COOH stretching vibrations in lauric acids, C – C=O stretching vibrations in quercetin, and D – CH_2 bending vibrations in lauric acid.

In order to analyze the spectra, the ratio of B to D peak area was calculated for the unloaded particles, 5% QE, 10% QE, and 20% QE. The ratio changed slightly, so it was concluded that the presence of quercetin does not affect the formation of new bonds in lauric acid.

In the next step, the ratio of B to C peak area was calculated for 5% QE, 10% QE, and 20% QE. This allowed us to determine whether the amount of quercetin in the particles is increasing. The ratio decreased with increasing quercetin concentration in the particles, so it was found that, as expected, the amount of encapsulated quercetin increases with increasing concentration in reaction mixture during microparticles preparation. Calculated ratios are shown in TABLE 1.

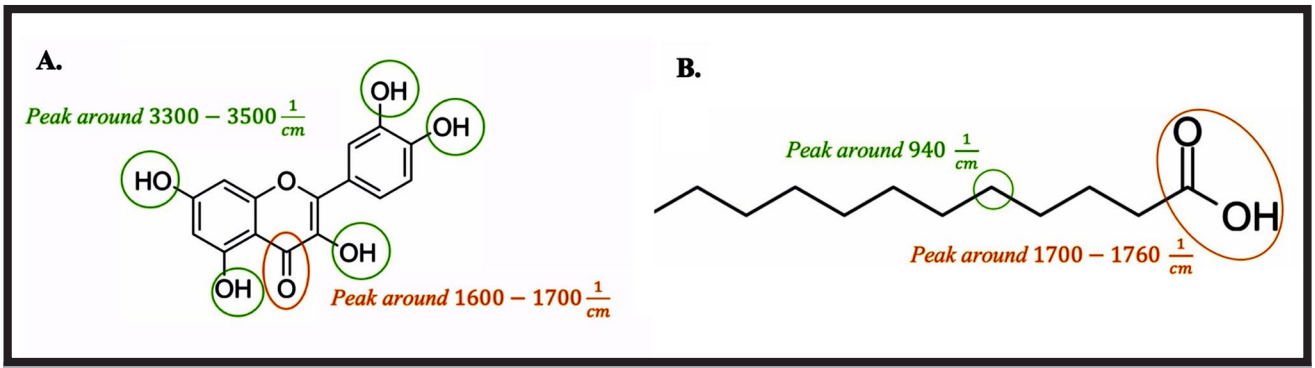

FIG. 5. The most characteristic bonds of A. quercetin and B. lauric acid and their FTIR peak position.

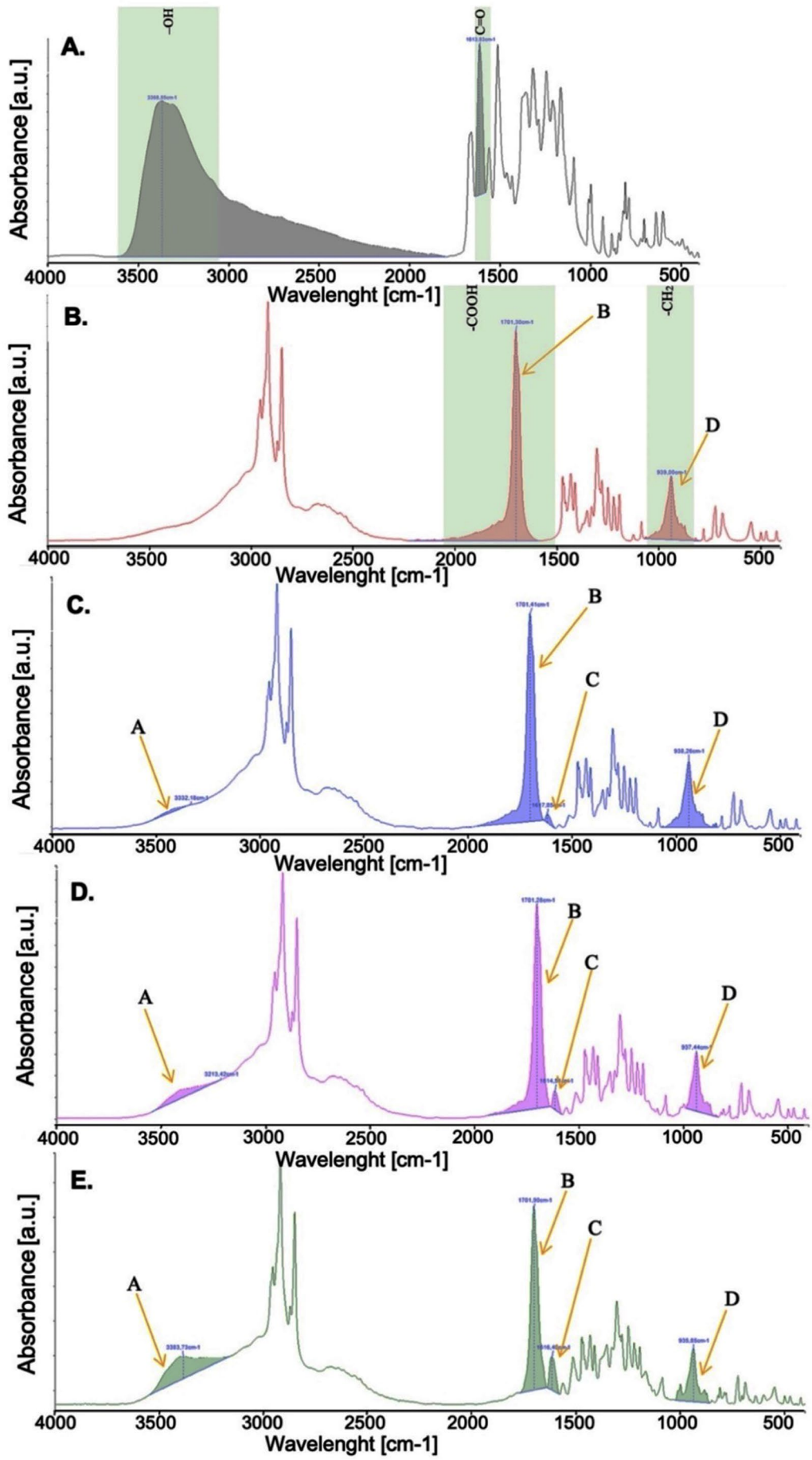

FIG. 6. FTIR spectra of manufactured particles and pure quercetin: A. unloaded particles, B. pure quercetin, C. loaded with 5% QE, D. loaded with 10% QE, E. loaded with 20% QE.

TABLE 1. The ratio of quercetin to lauric acid peaks indicating increasing encapsulation efficiency and ratio of lauric acid to lauric acid peaks as a validation of the absence of significant reactions between quercetin and lauric acid.

Concentration of QE in particles	Ratio of LAU : QE peaks	Ratio of LAU : LAU peaks
Unloaded	-	3.3:1
5%	24.5:1	3.2:1
10%	11.1:1	3.4:1
20%	5.6:1	3.5:1

Cytotoxicity test

To assess the ability of the particles to affect macrophage cytotoxicity, the LDH assay was performed.

The assay was performed for unloaded particles at 0.15 mg/ml concentration, quercetin powder at a concentration of 0.15 mg/ml, and quercetin-loaded microparticles at a concentration of 0.15 mg/ml and 0.30 mg/ml. The results from three independent donors are presented in FIG. 7.

The result showed that incubation with developed QE-loaded particles resulted in a higher percentage of LDH release for cells than unloaded particles; however, these values are distributed below the cytotoxicity threshold, which proves that QE-loaded particles were not cytotoxic for human macrophages.

To validate the significance of our findings, a statistical analysis was conducted. This analysis involved performing a t-test to compare the concentrations of quercetin (QE) within microparticles (MPs_QE0.15 and MPs_QE0.30) against microparticles without quercetin (MPs), as well as comparing QE alone against MPs. The results, as presented in TABLE 2, detail the t-test values and corresponding p-values for each comparison. Our analysis reveals a statistically significant distinction between both types of quercetin-loaded microparticles and unloaded microparticles. However, no significant differences were observed between the presence of QE alone and the unloaded microparticles.

Influence of quercetin on macrophage morphology

To assess macrophage morphology, cell nuclei and f-actin filaments were stained using DAPI and fluorescently labeled phalloidin-594, respectively. Fluorescence microscopy pictures were taken to analyze cells in terms of changes in morphology (FIG. 8).

Morphological differences were observed between cells incubated with quercetin (both encapsulated and pure substance) and unloaded particles when compared to the control group (primary human cells without stimulus – in the form of particles, pure active substance, or LPS). Macrophages incubated with unloaded particles and the control group had a small round-shaped morphology. However, cells exposed to quercetin were more spread and flattened. It can suggest that quercetin has an effect on macrophage morphology, causing their activation. Nonetheless, some research proved that M2 macrophages demonstrate a more spread morphology and have a larger size than the M1 phenotype [19]. Further research is needed to get a better insight into this matter. In this case, immunohistochemistry with the use of antibodies specific to M1 and M2 phenotypes could be advantageous.

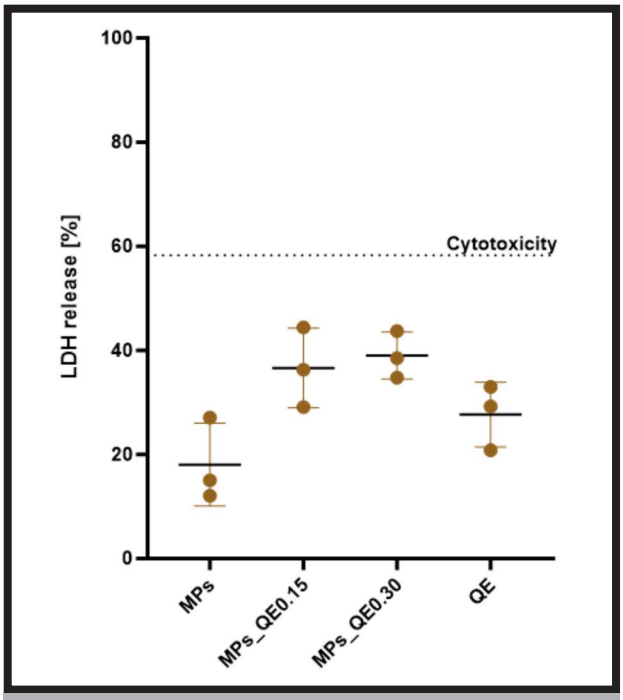

FIG. 7. Percentage of LDH released by macrophages from three different donors for: unloaded particles at a concentration of 0.15 mg/ml (MPs), particles loaded with quercetin at 0.15 mg/ml concentration (MPs_QE0.15), particles loaded with quercetin at 0.30 mg/ml concentration (MPs_QE0.30), and pure quercetin at a concentration 0.15 mg/ml (QE) after a 24 h incubation time. $n_{samples}$ = 3 per condition, p = 0.043 (one-way ANOVA). Statistical analysis including mean value and standard deviation.

TABLE 2. Statistical analysis of LDH release results including t-test, and corresponding p values, aimed to state the significance of the difference between the tested conditions.

	MPs_QE0.15	MPs_QE0.30	QE
MPs	t = 2.912, df = 4 p = 0.0436	t = 3.972, df = 4 p = 0.0165	t = 1.647, df = 4 p = 0.175

Visual inspection of nuclei staining has not shown significant differences in cells exposed to quercetin. The cell nuclei were round, of a similar shape, and stained with a similar intensity. These features indicate a lack of harmful effect of quercetin on nuclei morphology. The most significant differences in cytoskeleton staining can be observed between cells without stimuli (FIG. 8A) and MPs_QE0.30 (FIG. 8D). Cells in contact with a higher amount of QE-loaded microparticles were more spread and had more developed cytoskeleton fibers, similar to those cultured in contact with pure QU powder (FIG. 8E).

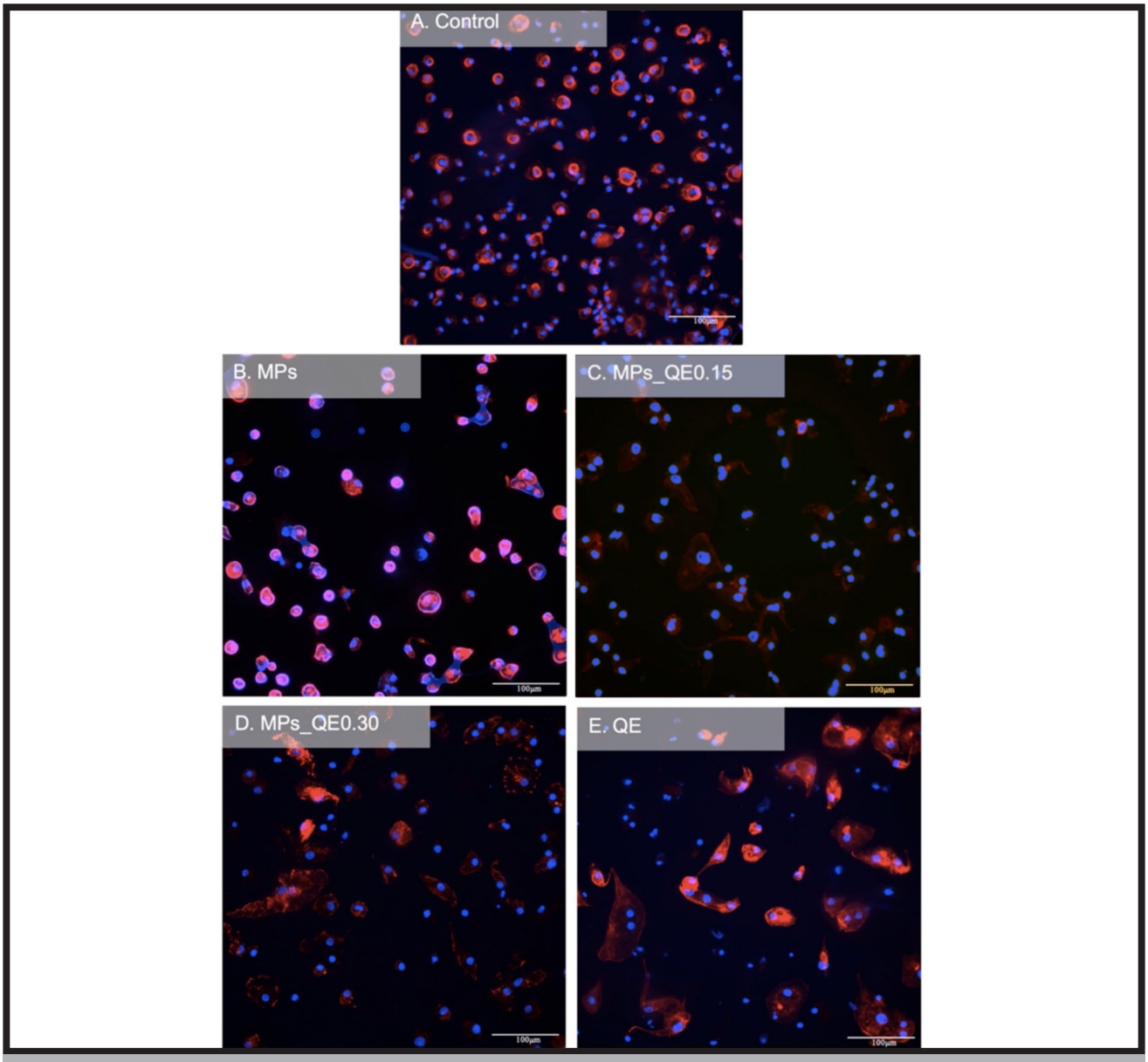

FIG. 8. Fluorescence microscopy images of DAPI/phalloidin staining of macrophages incubated for 24 h with the microparticles: cells without stimuli (Control) (A) and with: unloaded particles at a concentration of 0.15 mg/ml (MPs) (B), QE loaded particles at 0.15 mg/ml concentration (corresponding to 0.0075 mg/ml QE) (C), QE loaded particles at 0.30 mg/ml concentration (corresponding to 0.015 mg/ml QE) (D), and pure quercetin at 0.15 mg/ml concentration (E). Scale bar = 100 µm.

Influence of quercetin on macrophage polarization

Macrophages play a crucial role in directing inflammation due to their plasticity. Therefore, the ability of the particles to affect macrophage polarization was explored by flow cytometry for cells obtained from two donors. It was hypothesized that incubation with QE-loaded particles will influence the polarization state of macrophages. In FIG. 9, differences in dot plots can be observed between different conditions. Forward Scatter (FSC) and Side Scatter (SSC) in flow cytometry are providing information about the size and granularity of cells. However, activated or apoptotic cells might exhibit alterations in size or granularity, leading to shifts in their positions on the dot plot. Based on that, differences between dot plots in FIG. 9 might suggest that macrophages in different conditions exhibit different polarization states. Nevertheless, further research is necessary to study the influence of quercetin on the polarization state of macrophages.

Discussion

Quercetin is a naturally occurring flavonoid compound that has anti-inflammatory and anti-oxidant properties, dependent on numerous mechanisms. Taking into account the ability of quercetin to fight ROS and modulate inflammatory responses, it can be considered beneficial in the treatment of various diseases. Apart from its own anti-inflammatory mechanisms, this flavonoid can modulate actions of various immune cells, such as, e.g., macrophages, by influencing RNA transcription, antioxidant enzyme activity, and upregulating mitochondrial membrane potential. All of these actions result in a phenotypic change in macrophages, from an inflammatory phenotype to an anti-inflammatory phenotype [20,21]. Other research also shows quercetin suppressing effect on macrophage apoptosis pathways [22].

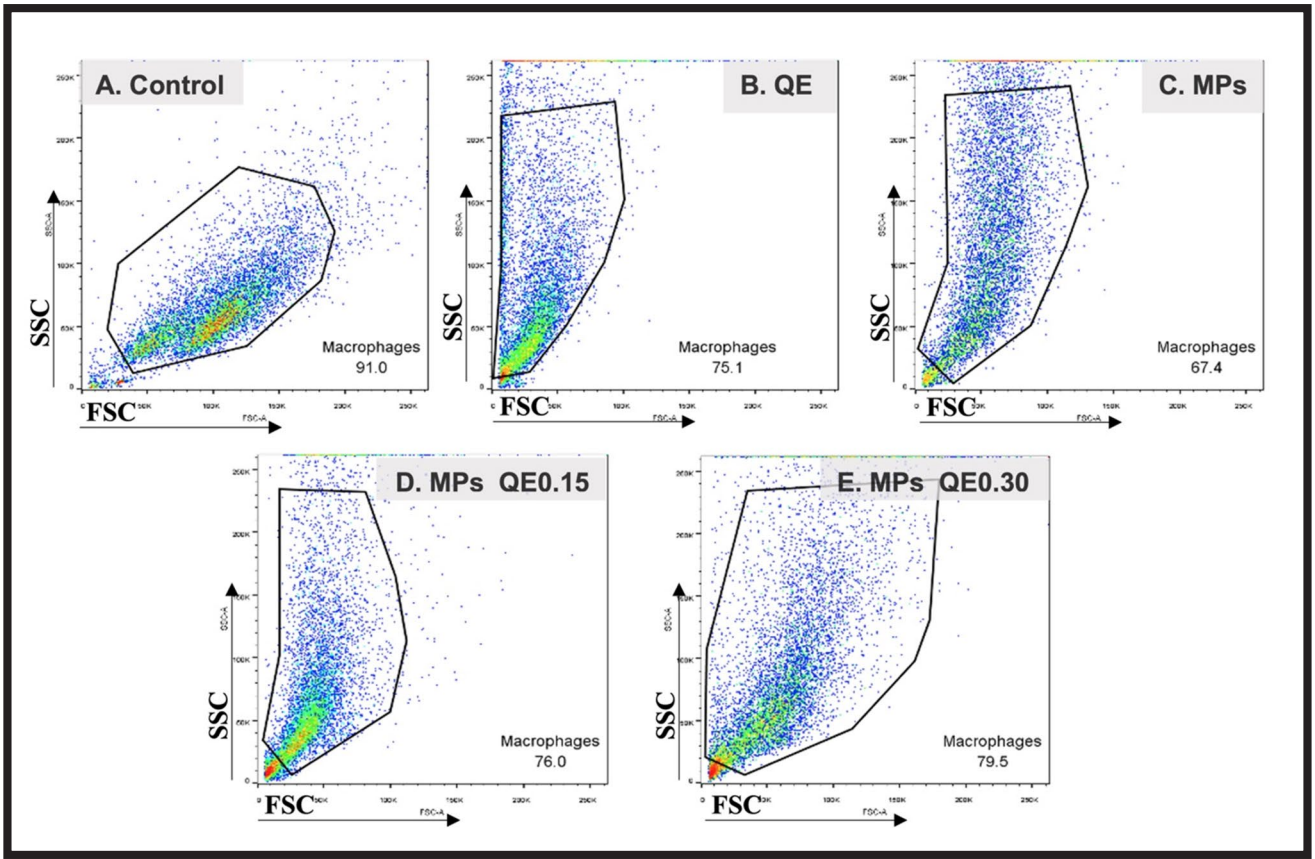

FIG. 9. Size and granularity of macrophages after 48 h of incubation with particles and pure active substance. Representative dot plots showing the aspect ratio.

In order to find agents supporting the burn wound healing process, lipid quercetin-loaded particles were produced and evaluated in terms of morphology, physicochemical properties, and biological capacity to affect macrophage viability and polarization. The manufacture of particles by the hot emulsification method guaranteed an average production efficiency of 46.5%. Moreover, the obtained particles presented a rounded shape and a defined size in a homogeneous final solution. On average, almost 60% of the particles had diameters less than 2 μm, which is advantageous due to the targeted use of the particles on skin wounds.

FTIR analysis confirmed the presence of quercetin and encapsulation efficiency in the lipid microparticles. It has been proven that no reactions occur between quercetin and lauric acid, by analyzing the area ratios between lauric acid:lauric acid characteristic peaks, which have retained their value. Furthermore, the are ratios between lauric acid:quercetin characteristic peaks allowed us to conclude that there was a decrease in these ratios when the concentration of quercetin increased, meaning that loading of quercetin in the particles is also increasing. To obtain the percentage values of loading efficiency, nuclear magnetic resonance (NMR) can be used in the future.

Lack of cytotoxicity of the manufactured particles and the necessity of encapsulation QE were proven by conducting LDH release assay. Adjusted concentrations of encapsulated and nonencapsulated active substance did not show a cytotoxic effect on macrophages after 24 h. Statistical analysis of our results confirmed a significant difference between encapsulated quercetin and unloaded microparticles. However, such a distinction was not observed between microparticles and quercetin alone. Nevertheless, encapsulation of the substance is essential to regulate the rate, time, and place of active substance release in drug delivery systems.

Macrophage morphology after incubation with microparticles and QE alone was also assessed through the staining of cells cytoskeleton and nuclei. The nuclei were round, with a similar shape, under all conditions. Moreover, differences between cells exposed to QE and incubated without QE were observed. Macrophages not exposed to QE can be described as small and round-shaped, while those exposed to QE non-encapsulated and encapsulated were more spread, flattened, and larger. These changes may be due to cell activation toward M2 macrophage phenotype as shown by others [23]. Further research would be needed to get a deeper insight into this observation. In this case, immunohistochemistry with the use of antibodies specific to M1 and M2 phenotypes could be advantageous.

The influence of QE on macrophage polarization was explored by flow cytometry. An evaluation was made for two healthy donors. As expected, a high number of CD14 expression levels were observed (data not shown). The inclusion of CD14 staining serves as a quality control measure for the experiment. Changes in size and granularity of macrophages under different conditions were observed, which might be due to differences in the activation state of the studied cells. However, to determine whether QE-loaded particles modulate polarization of macrophages, flow cytometry with the use of specific for macrophages subpopulations antibodies would have to be performed. To test the usefulness in fighting inflammation of the encapsulated material, further tests are needed to be performed, with particular emphasis on studying the release of quercetin from the particles and correlating them with macrophages polarization.

Conclusions

The production of lipid microparticles by the hot emulsification method allowed us for the encapsulation of quercetin, with increasing loading of the active substance by increasing the concentration of quercetin (5%, 10% and 20%) in the system during preparation. The presence of quercetin in the microparticles was confirmed by FTIR spectroscopy. The carriers were produced with a sufficient production efficiency of favorable shape and a median size in the range of 1.62-2.16 μm. Moreover, *in vitro* macrophage response for quercetin-loaded lipid microparticles was assessed. The particles did not show negative effects on macrophage morphology, as observed by the analysis of fluorescence images of DAPI-phalloidin red stained cells, although the cells in contact with pure quercetin and quercetin-loaded microparticles were more spread, which suggests their activations or polarization toward the anti-inflammatory (M2) phenotype. The carriers were found to be nontoxic to the cells, as shown by the LDH assay. The study used flow cytometry to examine the influence of quercetin on macrophage polarization, indicating potential changes in macrophage activation states. Further flow cytometry with specific antibodies for macrophage subpopulations is necessary to confirm the modulatory effect.

Overall, the obtained results show the potential of quercetin loaded lipid microparticles to combat inflammation and modulate burned skin regeneration.

Acknowledgements

This study was supported by the subsidy (No 16.16.160.557) for the AGH University of Krakow and the program Norte Regional Operational Program, Portugal – Structured R&D&I Projects – Unorte.pt. HEALTH-UNORTE; NORTE-01-0145-FEDER-000039 for the i3s Institute in Porto.

ORCID iD

J. Stępień: https://orcid.org/0009-0002-4002-3373
A. Kusibab: https://orcid.org/0000-0002-5580-7392
A.B. Sousa: https://orcid.org/0000-0002-3460-0499
J. Novais Barbosa: https://orcid.org/0000-0003-1852-2790
E. Pamuła: https://orcid.org/0000-0002-0464-6189

References

[1] H.N. Wilkinson, M.J. Hardman: Wound healing: cellular mechanisms and pathological outcomes: Cellular Mechanisms of Wound Repair. Open Biology 10(9) (2020), doi: 10.1098/rsob.200223.
[2] G. Broughton, J.E. Janis, C.E. Attinger: The basic science of wound healing. Plastic and Reconstructive Surgery 117(7) (2006). doi: 10.1097/01.prs.0000225430.42531.c2.
[3] P.H. Wang, B.S. Huang, H.C. Horng, C.C. Yeh, Y.J. Chen: Wound healing. Journal of the Chinese Medical Association 81(2) (2018) 94-101, doi: 10.1016/j.jcma.2017.11.002.
[4] A. Ridiandries, J.T.M. Tan, C.A. Bursill: The role of chemokines in wound healing. International Journal of Molecular Sciences 19(10) (2018). doi: 10.3390/ijms19103217.
[5] M. Rodrigues, N. Kosaric, C.A. Bonham, G.C. Gurtner: Wound Healing: A Cellular Perspective. Physiol Rev 99 (2019) 665-706, doi: 10.1152/physrev.00067.2017.-Wound.
[6] K.S. Smigiel, W.C. Parks: Macrophages, Wound Healing, and Fibrosis: Recent Insights. Current Rheumatology Reports 20(4) (2018), doi: 10.1007/s11926-018-0725-5.
[7] M.G. Jeschke, M.E. van Baar, M.A. Choudhry, K.K. Chung, N.S. Gibran, S. Logsetty: Burn injury. Nat Rev Dis Primers 6(1) (2020), doi: 10.1038/s41572-020-0145-5.
[8] M.G. Jeschke, L.-P. Kamolz, F. Sjöberg, S.E. Wolf: Handbook of burns – Acute burn care. SpringerWienNewYork, Vol. 1, (2012), doi:10.1007/978-3-7091-0348-7
[9] L. Rae, P. Fidler, N. Gibran: The Physiologic Basis of Burn Shock and the Need for Aggressive Fluid Resuscitation. Critical Care Clinics 32(4) (2016) 491-505, doi: 10.1016/j.ccc.2016.06.001.
[10] C.B. Nielson, N.C. Duethman, J.M. Howard, M. Moncure, J.G. Wood: Burns: Pathophysiology of Systemic Complications and Current Management. Journal of Burn Care and Research 38(1) (2017) e469-e481, doi: 10.1097/BCR.0000000000000355.
[11] J.A. Snell, N.-H.W. Loh, T. Mahambrey, K. Shokrollahi: Clinical review: The critical care management of the burn patient. Critical care 17(5) (2013) 241. doi: 10.1186/cc12706.
[12] M.G. Jeschke, S. Shahrokhi, C.C. Finnerty, L.K. Branski, M. Dibildox: Wound Coverage Technologies in Burn Care: Established Techniques. Journal of Burn Care and Research 39(3) (2018) 313-318, doi: 10.1097/BCR.0b013e3182920d29.
[13] W. Shu, Y. Wang, X. Zhang, C. Li, H. Le, F. Chang: Functional Hydrogel Dressings for Treatment of Burn Wounds. Frontiers in Bioengineering and Biotechnology 9 (2021), doi: 10.3389/fbioe.2021.788461.
[14] H. Memariani, M. Memariani, A. Ghasemian: An overview on anti-biofilm properties of quercetin against bacterial pathogens. World Journal of Microbiology and Biotechnology 35(9) (2019), doi: 10.1007/s11274-019-2719-5.
[15] T. Hatahet, M. Morille, A. Hommoss, J.M. Devoisselle, R.H. Müller, S. Bégu: Quercetin topical application, from conventional dosage forms to nanodosage forms. European Journal of Pharmaceutics and Biopharmaceutics 108 (2016) 41-53, doi: 10.1016/j.ejpb.2016.08.011.
[16] V. Kant, B.L. Jangir, V. Kumar, A. Nigam, V. Sharma: Quercetin accelerated cutaneous wound healing in rats by modulation of different cytokines and growth factors. Growth Factors 38(2) (2020) 105-119, doi: 10.1080/08977194.2020.1822830.
[17] D. Yang, T. Wang, M. Long, and P. Li: Quercetin: Its Main Pharmacological Activity and Potential Application in Clinical Medicine. Oxidative Medicine and Cellular Longevity (2020). Hindawi Limited, doi: 10.1155/2020/8825387.
[18] Y. Li et al.: Quercetin, inflammation and immunity. Nutrients 8(3) (2016), doi: 10.3390/nu8030167.
[19] W. Wang, K.J. Lu, C.H. Yu, Q.L. Huang, Y.Z. Du: Nano-drug delivery systems in wound treatment and skin regeneration. Journal of Nanobiotechnology 17(1) (2019), doi: 10.1186/s12951-019-0514-y.
[20] H.M. Rostam, P.M. Reynolds, M.R. Alexander, N. Gadegaard, A.M. Ghaemmaghami: Image based Machine Learning for identification of macrophage subsets. Sci Rep 7(1) (2017), doi: 10.1038/s41598-017-03780-z.
[21] C.-F. Tsai, G.-W. Chen, et. al.: Regulatory Effects of Quercetin on M1/M2 Macrophage Polarization and Oxidative/Antioxidative Balance. Nutrients. 14(1):67 (2022).
[22] X. Luo, X. Bao, et. al.: The protective effect of quercetin on macrophage pyroptosis via TLR2/Myd88/NF-κB and ROS/AMPK pathway. Life Science 291 (2022).
[23] J. Peng, Z. Yang, H. Li, B. Hao, et al.: Quercetin Reprograms Immunometabolism of Macrophages via the SIRT1/PGC-1α Signaling Pathway to Ameliorate Lipopolysaccharide-Induced Oxidative Damage. International Journal of Molecular Science 24 (2023) 5542.

EXAMINATION OF STRENGTH PROPERTIES OF THE TEMPOROMANDIBULAR JOINT DISC

Agnieszka Szust[1], Anna Wybraniec[1], Gabriela Wielgus[1,2*]

[1] Wrocław University of Science and Technology, Faculty of Mechanical Engineering, Department of Mechanics, Materials and Biomedical Engineering, Wybrzeże St. Wyspiańskiego 27, 50-370 Wrocław, Poland
[2] Silesian University of Technology, Faculty of Biomedical Engineering, Akademicka 2A, 44-100 Gliwice, Poland
*e-mail: gw309118@student.polsl.pl

Abstract

The purpose of this research was to determine selected biomechanical properties of the temporomandibular disc. After endurance tests and once the load-displacement characteristics were determined, the susceptibility and dimensionless energy dissipation coefficient were determined. The research was carried out on ten discs (six fresh and four frozen) taken from five young pigs. Endurance tests were conducted in the laboratory of Wrocław University of Science and Technology, using the INSTRON 5944 machine. All tested discs were kept in a NaCl solution heated to 37.5ºC during the experiment. A recurring difference of 1 mm in the height of the fresh and frozen discs was observed. In contrast, the strength of the discs was similar regardless of the method of storing the preparation. The material susceptibility values ranged from 0.4 to 1.4 millimetre per Newton, and the dimensionless energy dissipation factor oscillated between 0.27 and 0.87.

The aim of these experimental investigations was to determine the compressive force at predefined strain levels and to elucidate the loading characteristics corresponding to displacement. Due to the observed variability in these characteristics across consecutive measurement cycles, the analysis in this paper is restricted to the results obtained from the first measurement series.

Keywords: *temporomandibular joint disc, biomechanical properties, dimensionless energy dissipation factor, susceptibility*

Introduction

The temporomandibular joint is considered the most complex joint in the human body both functionally and anatomically. The temporomandibular joint is the only paired joint and the only mobile joint, a true joint, in the craniofacial region. Therefore, the functional anatomy and biomechanics of this joint are extremely complex. The disc in the temporomandibular joint is classified as a hinge position joint, which means that it allows hinged movement in one plane and translational movements. With this combination of movements, it is possible to open and close the mouth and move the mandible in different directions [1].

The functional and anatomical complexity of the temporomandibular joint often results in various dysfunctions. These are congenital, developmental, and acquired as a result of conditions such as neck muscle contractures, postural defects, or malocclusion, for example. As a result of these dysfunctions and damage from trauma, disc damage and inflammatory or degenerative conditions can occur [2-5].

Despite the important role of the temporomandibular joint in anatomy and function, many questions about its biomechanics and adaptation in different conditions remain unclear. Most studies are based on research material collected from animals, and, in particular, pigs [6-11]. Porcine anatomy has a high convergence with human anatomy, making it a suitable model for the study of the temporomandibular joint and other anatomical structures [12]. Taking this into account, the authors of this thesis decided to conduct an experimental strength study using pig temporomandibular joint discs.

Materials and Methods

The study material consisted of the temporomandibular joint of pigs aged between 4 and 6 months. The discs were collected immediately after the head of the pig was delivered to the laboratory. After the discs were taken from the pig's head, the biological material was tested for strength, or frozen until testing (FIG. 1). Each time before the strength tests, the discs were visually assessed for mechanical damage or other defects that would disqualify the testing value of the sampled material. The dimensions of the discs were then measured.

Based on thickness measurements, the amount of strain understood as the change in disc height at the central point of the surface was determined (FIG. 2) [9]. Thanks to these measurements, it was possible to properly adjust the strength test conditions to the specific parameters of the biological material tested, which was crucial to the correctness and precision of the tests carried out.

After taking all the necessary measurements, the temporomandibular joint discs were subjected to a compression test. The test was carried out using the INSTRON 5944 testing machine, equipped with a 2 kN actuator (FIG. 3). The tests were carried out in an aqueous environment - 90% NaCl heated to 37.5°C, using a vessel for this solution. The discs were subjected to a compression test, loading the centre of the disc with force, resulting in a change in height corresponding to a relative deformation of 80% of the height.

[Engineering of Biomaterials 171 (2023) 12-17]

doi:10.34821/eng.biomat.171.2023.12-17

Submitted: 2023-10-16, Accepted: 2023-11-20, Published: 2023-11-22

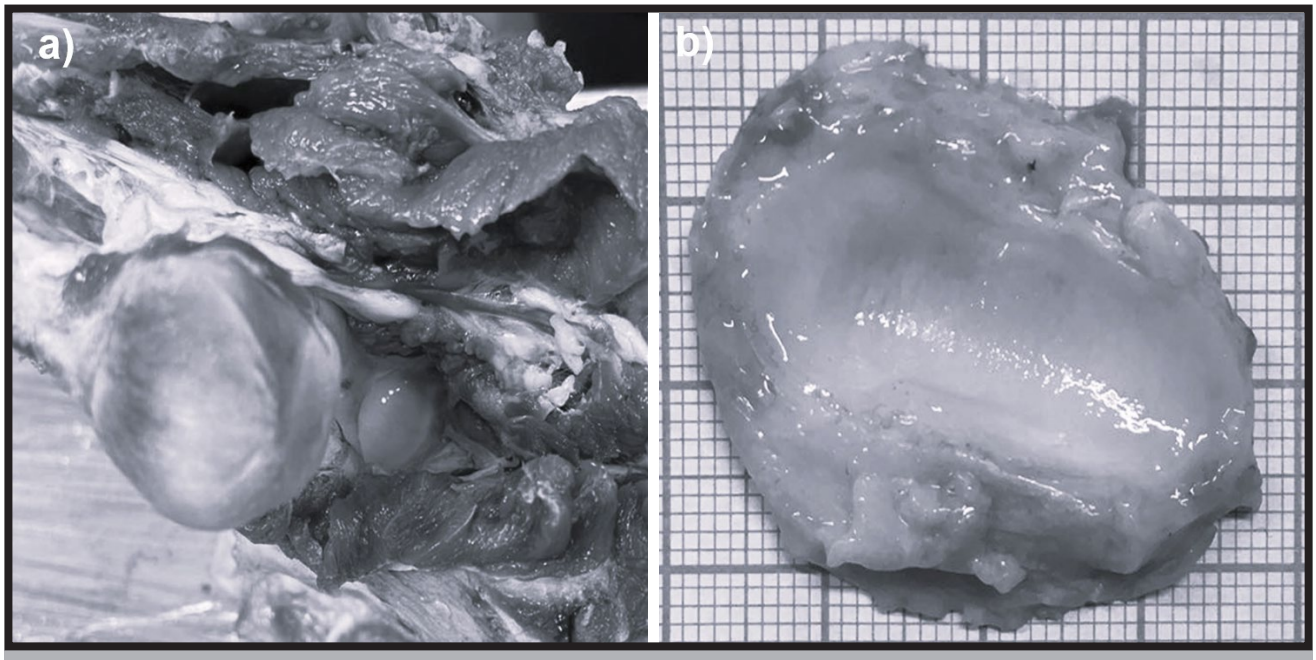

FIG. 1. a) Process of preparing the material for the endurance testing disc in the porcine temporomandibular joint before preparation, b) prepared test specimen - the temporomandibular joint disc.

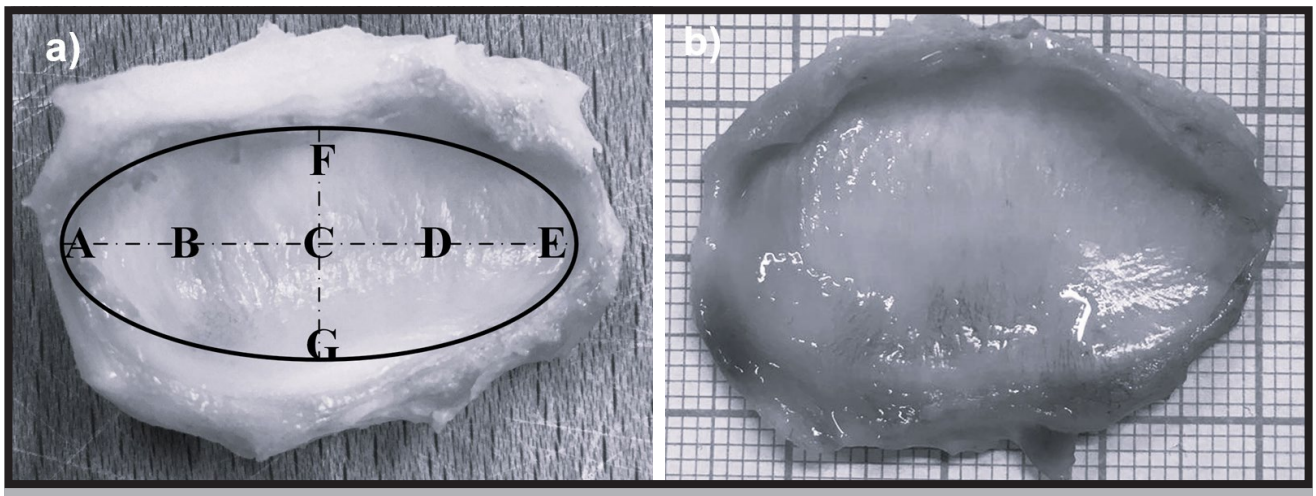

FIG. 2. a) Diagram with marked zones for measuring the thickness of the temporomandibular joint disc from the cranial side - before examination, b) the temporomandibular joint disc from the mandibular side - before examination.

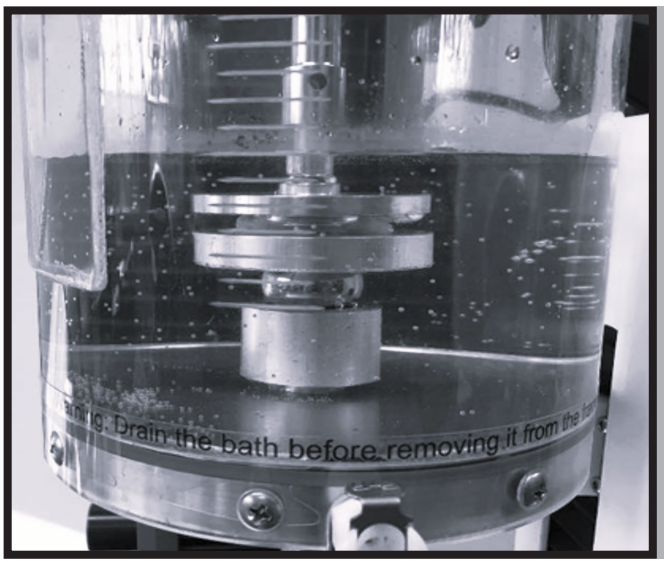

FIG. 3. Test stand for endurance tests, with the temporomandibular joint disc preparation to be tested, in holding wraps, in a saline bath at 37.5°C.

All tests were carried out under the same conditions, using the following procedure: in the first minute, the temporomandibular joint disc was loaded with a force to reach 80% of its height; in the second minute of measurements, the disc was compressed by the testing machine at a constant displacement of the actuator in the last minute of each measurement series, the disc was relaxed, i.e. relieved of load (each test consisted of three series of measurement) [12] - after the experiment was performed, the load-displacement characteristics were obtained. Subsequently, a strength test analysis was carried out to determine the compressive deformation susceptibility of the material (the compressive stiffness of the puck was not determined because the governing formula is applied using Hooke's law, which does not apply when testing on biological material). The susceptibility was determined from the first measurement test.

$$S_c = u/F_c \text{ [mm/N]}$$

u - displacement [mm],
F_c - compressive force [N].

On the basis of the results obtained, hysteresis loops were determined (based on the approximation of the diagram) to determine the dimensionless energy dissipation factor. The dimensionless energy dissipation factor was determined on the basis of the first measurement attempt.

$$\Psi = A_H/A_S$$

A_S - field under the graph,
A_H - hysteresis surface area.

After the strength test, the geometry of each disc was re-measured.

Results and Discussions

Six discs were selected for the analysis of the results, four of which were fresh and two of which had undergone a freezing process. This decision was made in order to eliminate incorrect measurement data, raising doubts about the other materials collected. The designations of the test samples are summarized in TABLE 1.

Before and after the compressive strength test, the width and height of the discs were measured to observe the geometric changes of the test material. The results of the geometric disc measurements are shown in TABLE 2 and in FIGs 4 and 5.

TABLE 1. Designation of test samples.

Sample	Temporomandibular joint disc
k.1	frozen
k.2	fresh
k.3	fresh
k.4	frozen
k.5	fresh
k.6	fresh

TABLE 2. Geometric dimensions of the articular disc from the cranial side before and after examination.

Sample	width of the temporomandibular joint disc [mm]		height of the temporomandibular joint disc [mm]	
	before the test	after the test	before the test	after the test
k.1	27.9	28.2	17.4	16.9
k.2	28.2	28.7	17.9	17.1
k.3	30.5	30.9	17.9	17.2
k.4	31.8	31.2	18.5	18.3
k.5	28.8	29.2	21.0	19.8
k.6	26.1	27.1	18.4	15.6
results	(28.9±2.0)	(29.2±1.6)	(18.5±1.3)	(17.5±1.4)

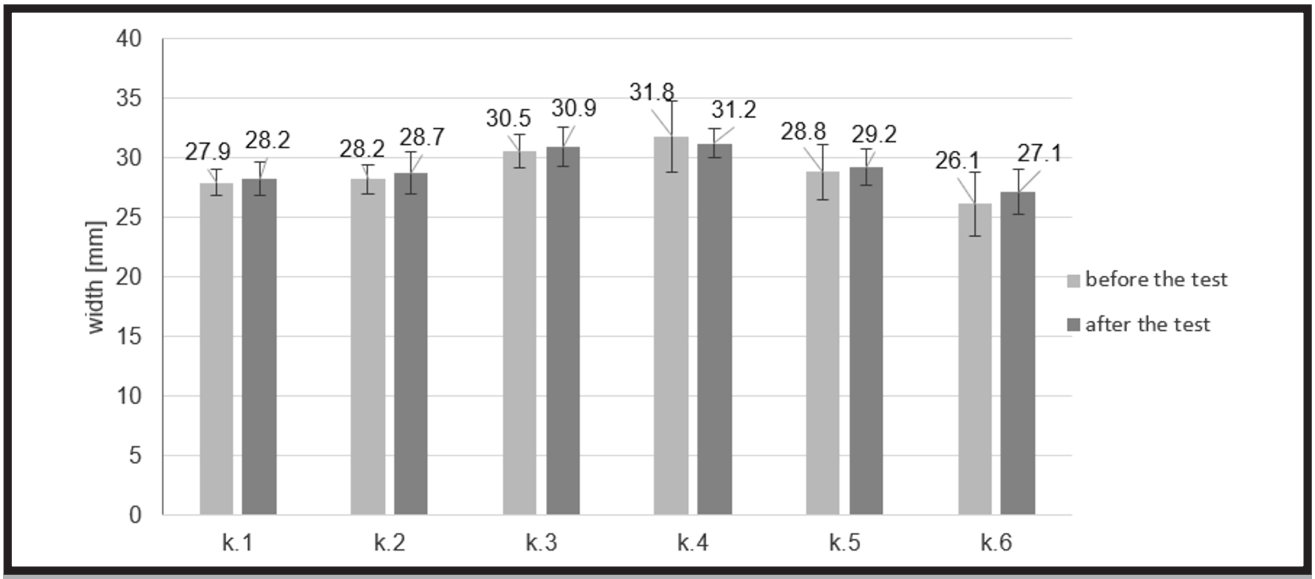

FIG. 4. Width of the temporomandibular joint disc before and after the test.

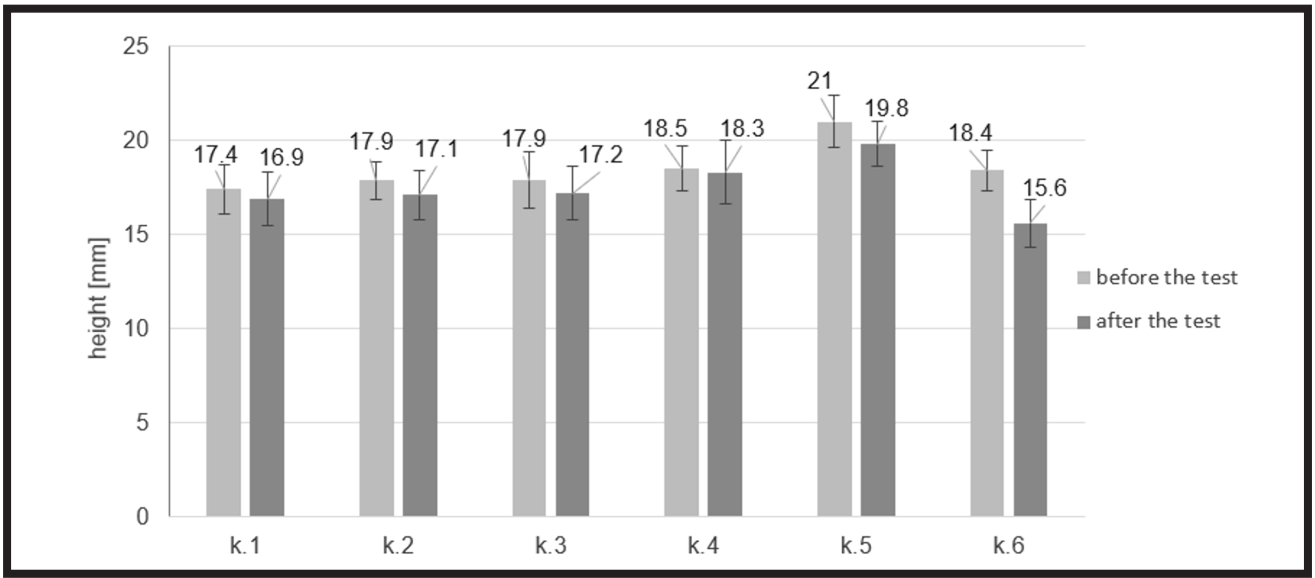

FIG. 5. Height of the temporomandibular joint disc before and after the test.

The results of the pre- and post-test disc thickness measurements were collected as mean values along with the standard deviation (TABLE 3). The key measurement was the central area, marked C, which was subjected to further strength testing. The thickness of the discs was also measured after the experiments to observe any differences.

The results of the maximum temporomandibular joint disc load measurements for each first measurement trial were collected and presented in TABLE 4. Load-displacement characteristics was determined for each temporomandibular disc tested (FIG. 6).

The results of the maximum susceptibility values of the discs for the first measurement test are summarized in TABLE 5.

A dimensionless energy dissipation coefficient was then determined, understood as a measure of energy loss during cyclic loading, which reflects the material's ability to absorb energy during deformation and resist fracture. Analysis of this coefficient allows the strength of the material and its behaviour under dynamic conditions to be assessed.

TABLE 3. Measurement of the thickness of the temporomandibular joint disc.

Sample	before the strength test [mm]						
	A	B	C	D	E	F	G
k.1	0.09±0.02	0.97±0.01	0.86 ±0.01	0.94 ±0.01	0.93±0.02	1.31±0.04	2.63±0.01
k.2	0.64±0.01	1.00±0.02	1.06 ±0.01	0.89±0.01	1.10±0.02	3.40±0.01	2.35±0.02
k.3	0.94±0.04	0.74±0.01	0.76±0.01	0.59±0.01	1.20 ±0.01	3.90±0.01	3.33±0.01
k.4	1.17±0.02	1.14±0.03	1.06 ±0.02	1.31±0.02	1.07±0.02	3.13±0.04	4.5±0.02
k.5	0.79±0.01	0.61±0.01	0.92±0.01	0.91±0.02	0.86±0.01	2.01±0.03	2.09±0.01
k.6	1.01±0.01	0.76±0.01	1.00±0.01	0.82±0.01	0.82±0.01	3.72±0.03	3.44±0.01
	after the strength test [mm]						
k.1	1.56±0.03	1.06±0.02	0.99±0.02	1.21±0.01	0.99 ±0.03	1.13±0.02	3.20±0.08
k.2	1.01±0.02	1.04±0.01	1.19±0.02	1.03±0.02	0.87±0.02	2.59±0.01	1.74±0.03
k.3	1.36±0.02	1.68±0.01	1.75±0.01	0.93±0.02	1.18±0.01	2.94±0.02	3.46±0.02
k.4	1.16±0.13	0.96±0.02	1.25±0.02	1.21±0.01	1.12±0.02	3.70±0.04	3.09±0.02
k.5	0.97±0.01	1.01±0.01	0.71±0.01	0.55±0.01	0.82±0.02	1.96±0.06	2.96±0.02
k.6	1.08±0.02	0.84±0.01	1.11±0.01	1.17±0.04	0.92±0.01	3.85±0.01	3.88±0.02

TABLE 4. Maximum load values.

Measurement series	k.1	k.2	k.3	k.4	k.5	k.6
	F_{cmax} [N]					
I	2.14	1.2	2.44	0.56	1.99	1.91
II	0.67	0.87	1.52	0.25	2.21	0.35
III	0.50	0.76	1.46	0.24	2.04	0.26

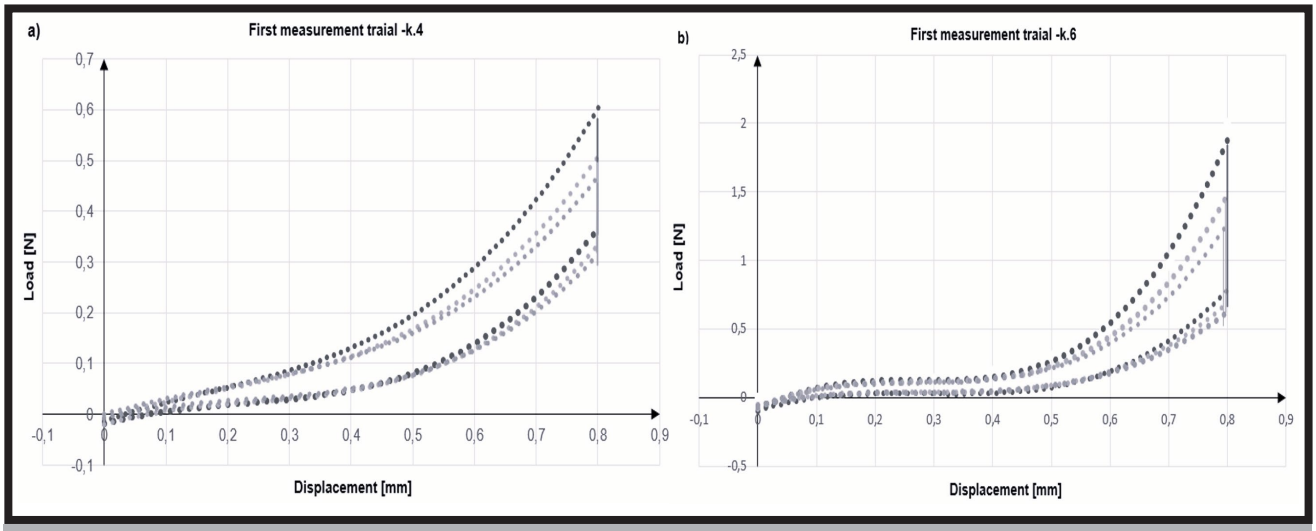

FIG. 6. Temporomandibular joint disc strength test: a) frozen disc, b) fresh disc.

TABLE 5. Maximum values for temporomandibular joint disc compliance.

Temporomandibular joint disc	S_c [mm/N]
k.1	0.37
k.2	0.67
k.3	0.33
k.4	1.43
k.5	0.40
k.6	0.42

TABLE 6. Dimensionless energy dissipation factor.

Sample	A_H	A_S	Ψ
k.1	0.18	0.24	0.76
k.2	0.18	0.38	0.48
k.3	0.25	0.29	0.87
k.4	0.02	0.10	0.21
k.5	0.08	0.15	0.56
k.6	0.06	0.23	0.27

The A_H parameter was determined by calculating the hysteresis area (TABLE 6). This analysis focuses on various aspects of the behaviour of the temporomandibular joint disc under load and the interpretation of the data obtained in terms of their clinical and biomechanical significance.

Geometric measurements of the temporomandibular joint discs from the cranial side were taken before strength testing. It was observed that frozen discs appeared slightly thicker than those freshly collected from pigs. However, it should be noted that this difference is not significant. The results of these measurements are shown in TABLE 2, where the values obtained differed by approximately ±1 mm.

When compression tests were carried out on the discs, slight changes were observed in the thickness of the discs. After the test, the width of the discs increased, while the height of the discs decreased. After three measurement series on a given disc, the second and third series were characterized by lower maximum load values, confirming the thesis of geometric changes in the disc. These differences are described in detail in TABLE 3. The width of the discs marked in FIG. 2a at points (A, B, D, E) increases, while their height at points (F and G) decreases. This is a predictable effect of the compression tests, which results in a flatter disc. The largest geometric changes have been observed for disc k.1, which is a frozen disc, and the smallest changes have been observed for the fresh disc, k.6. However, these differences are not relatively high between fresh and frozen discs.

In addition, based on geometry measurements, great similarity in the size of the human temporomandibular joint disc was observed - the thickness of the pig disc at point C of the disc k.1 is 0.86 mm, while the human disc according to [12] is 0.9 mm. This observation provides further confirmation of the validity of subletting experimental studies on pig discs.

Hysteresis plots were obtained for all samples tested, as described in this article. To correctly visualize the measurement data, a polynomial approximation of the trend line (3rd order) was used. Thus, it should be noted that the 'moduli' of the measurement series carried out grew non-linearly, clearly demonstrating the non-linear nature of the material. It has been observed that excessive compression of the disc is associated with permanent, invariant geometric changes [7].

In addition, the susceptibility of the discs was determined for each of the first measurement trials, the values obtained for which are shown in TABLE 5. The susceptibility values of the material ranged from ±0.4-1.4 mm/N. The relatively low susceptibility values may be due to the collection of material from young pigs between 4 and 6 months of age.

Subsequently, the dimensionless energy dissipation factor was also determined for each first measurement sample. This ratio, which is the ratio of the area of the hysteresis loop to the area under the graph, reached values oscillating between ±0.27 and 0.87, consistent with the data available in the literature [13]. It was found that the area under the hysteresis plot is related to the geometry of the temporomandibular joint disc and its storage method, i.e., whether it is fresh or frozen. The highest energy damping coefficient was recorded for the fresh disc marked k.3.

Conclusions

The experimental studies of the temporomandibular joint discs described in this work are pilot studies to determine how to proceed in strength testing for uniformity in the origin of biological material. The most important objective of these experimental studies was to determine the compressive force at a given strain and to determine and describe the characteristics of loading from displacement. Due to the variability of characteristics during successive measurement cycles, in this paper, the analysis of the results is presented only for the first measurement series [12]. During the strength tests, the values of the susceptibility Sc of the tested biological material and the dimensionless energy dissipation coefficient Ψ were determined. The results obtained do not differ from the typical results observed for tests on temporomandibular joint discs [13]. In the future, the overarching research objective for the authors is to present for a wider research sample the strength properties of the discs, which can serve as a source for both further experimental and analytical (FEM) studies.

Acknowledgements

This work was supported by a subvention from the Division of Biomedical Engineering and Experimental Mechanics, Wrocław University of Technology, Wrocław, Poland.

ORCID iD

A. Szust: https://orcid.org/0000-0002-6448-6703
A. Wybraniec: https://orcid.org/0000-0002-6947-2765
G. Wielgus: https://orcid.org/0009-0001-5180-5269

References

[1] Dołoszycka M., Kulesa-Mrowiecka M., Kopański Z., Krzemiński D., Ptak W., Dyl S., Sklyarov I.: Selected aspects of anatomy and biomechanics of the stomatognathic system. Journal of Public Health, Nursing and Medical Rescue 6 (2018) 1-4.
[2] Górecka M., Pihut M., Ferendiuk E.: Charakterystyka schorzeń stawów skroniowo-żuchwowych. Dental Forum XLIV(1) (2016) 63-67.
[3] Luo D., Yang Z., Qiu C., Jiang Y., Zhou R., Yang J.: A magnetic resonance imaging study on the temporomandibular joint disc–condyle relationship in young asymptomatic adults. Int. J. Oral Maxillofac. Surg. 51(2) (2022) 226-233.
[4] Pihut M., Wiśniewska G., Majewski S.: Odległe wyniki leczenia pacjentów z objawami patologicznego przemieszczenia krążka stawowego bez zablokowania. Protet. Stomatol. LXI(5) (2011) 419-425.
[5] Majewski S., Wieczorek A., Loster J., Pihut M.: Mięśnie żucia i stawy skroniowo-żuchwowe w aspekcie fizjologicznych funkcji układu stomatologicznego. Protet. Stomatol. LX(1) (2010) 10-16.
[6] Kajzer A., Kajzer W., Basiaga M., Kuna E.: Badania własności mechanicznych kości wołowych i wieprzowych. Inżynieria Biomateriałów 119 (2013) 45-50.
[7] Matuska A.M., Muller S., Dolwick M.F., McFetridge P.S.: Biomechanical and biochemical outcomes of porcine temporomandibular joint disc deformation. Osteoarthritis and Cartilage 17 (2009) 1408-1415.
[8] Murphy M.K., Arzi B., Hu J.C., Athanasio K.A.: Tensile Characterization of Porcine Temporomandibular Joint Disc Attachments. J Dent Res 92(8) (2013) 753-758.
[9] Wu Y., Kuo J., Wright G.J., Ciewski S.E., Wei F., Kern M.J., Yao H.: Viscoelastic shear properties of porcine temporomandibular joint disc. Orthod Craniofac Res 18(1) (2015) 156-163.
[10] Bermejo A., Gonzalez O., Gonzalez J.M.: The pig as an animal model for experimentation on the temporomandibular articular complex. Oral Surc Oral Med Oral Pathol 75 (1993) 18-23.
[11] Murphy M.K., Arzi B., Hu J.C., Athanasiou K.A.: Tensile Characterization of Porcine Temporomandibular Joint Disc Attachments. J Dent Res 92(8) (2013) 753-758.
[12] Chaldek W., Czerwika I.: Wpływ przecięcia tkanek na wyniki badań właściwości mechanicznych krążków stawu skroniowo żuchwowego. Inżynieria Biomateriałów 67-68 (2007) 16-18.
[13] Margielewicz J., Kijak E., Lipski T., Pihut M., Kosiewicz J., Lietz-Kijak D.: Badania modelowe równowagi biostatycznej narządu żucia człowieka. Centrum Inżynierii Biomedycznej, Gliwice (2012) 4-206.

COMPARATIVE ASSESSMENT OF INTRANASAL DRESSINGS MADE OF VARIOUS TYPES OF BIOMATERIALS, APPLIED AFTER FUNCTIONAL ENDOSCOPIC SINUS SURGERY

Azad Maou[1], Wirginia Likus[2], Anna Długosz-Karbowska[1], Jan Pilch[1], Jarosław Markowski[1]*

[1] Department of Laryngology,
Faculty of Medical Sciences in Katowice,
Medical University of Silesia in Katowice,
20-24 Francuska Str., 40-027 Katowice, Poland
[2] Department of Anatomy,
Faculty of Health Sciences in Katowice,
Medical University of Silesia in Katowice,
18 Medyków Str., 40-752 Katowice, Poland
*e-mail: jmarkow1@poczta.onet.pl

Abstract

The aim of the study was to make a comparative evaluation of four different types of intranasal dressings made from various types of biomaterials (three original dressings manufactured by various commercial suppliers, and the fourth one, in the form of nasal tamponage by means of a seton in a latex glove finger cot), concerning their efficacy as regards haemostatic action, assessment of postoperative pain, as well as proneness to the occurrence of postoperative adhesions.

All patients who were qualified for the study were operated on in the ENT Department, Medical University of Silesia in Katowice, Poland, due to chronic bilateral inflammation of the para-nasal sinuses, confirmed by computer tomography of the sinuses. A total of 180 patients were qualified for the study. After surgery, 4 different kinds of intranasal haemostatic dressings were applied. The results were analyzed in three categories: effectiveness in the field of haemostatic activity, postoperative pain assessment (Visual Analog Scale, VAS), and assessment of the tendency to develop postoperative adhesions.

Statistical analysis revealed no statistically significant differences between the 4 types of dressings in both haemostatic efficacy ($p = 0.97$) and the occurrence of postoperative adhesions ($p = 0.84$). Analysis of the intensity of pain according to the VAS scale indicated that it did not differ between the analyzed groups, both during the application of dressing (mild pain) and on the second day after the operation (medium intensity pain) – $p = 0.30$ and $p = 0.39$, respectively.

No advantage has been demonstrated for any of the 4 analysed types of intranasal haemostatic dressings over any other. Their properties turn out to be comparable.

[Engineering of Biomaterials 171 (2023) 18-22]

doi:10.34821/eng.biomat.171.2023.18-22

Submitted: 2023-11-02, Accepted: 2023-11-28, Published: 2023-12-01

Keywords: *carboxymetyllocelulose, polyvinyl alcohol, latex, intranasal dressings, functional endoscopic sinus surgery, postoperative care*

List of abbreviations:
EPOS – European Position Paper of Rhinosinustis and Nasal Polyps 2020
FESS – Functional endoscopic sinus surgery
NS – Nasal Sponge pack
MP – Merocelpope nasal dressing
RR – RapidRhino nasal dressing
RNP – Routine nasal pack

Introduction

Chronic rhinosinusitis affects between 5 and 15% of the total population in Europe [1]. Para-nasal sinusitis currently ranks as one of the 10 most common diseases. Therefore, chronic sinusitis is a medical and social problem. In today's medicine, functional endoscopic sinus surgery (FESS) is the gold standard for the treatment of chronic sinusitis; FESS is one of the most frequently performed operating procedures by otorhinolaryngologists [1]. In order to prevent the occurrence of complications in the form of postoperative bleeding, pain experienced during the removal of the internal dressing from the nasal cavities, and the development of adhesions in the nasal cavity, many techniques and dressing materials have been introduced; however, no ideal and widely accepted solution has been developed so far [2-13].

Although the use of endoscopes in operational techniques has introduced a new quality, both with regard to treatment results, as well as intraoperative safety, the most common complication of surgery performed in the area of para-nasal sinuses is postoperative bleeding, and pain associated both with the presence of a dressing in the nose itself, as well as pain developing during the procedure of dressing removal, and the development of adhesions [14-23]. For these reasons, more effective and patient-friendly techniques and nasal dressing materials are still being sought [17-24]. New soluble dressings, recently introduced into clinical practice, have been reported to be more comfortable for the patient [25-33].

The aim of the study was to perform a comparative assessment of four different types of intranasal dressings made of different biomaterials, three original dressings from different producers: NasalSponge® (MDD Medical Devices), MerocelPope® (Medtronic), RapidRhino® (Smith & Nephew), and the fourth type of dressing commonly used in the form of nasal tamponade seton soaked with antibiotic and steroid ointment in rubber glove finger made of latex. The comparative analysis of these 4 types of intranasal dressings was carried out from the perspective of their: (i) effectiveness of hemostatic effect, (ii) assessment of the level of postoperative pain during the application of the nasal dressing, (iii) the level of pain experienced during the removal of the intranasal dressing on the 2nd day after surgery, and (iv) assessment of the proneness to develop postoperative adhesions in the nasal cavities, assessed after 4 and 8 weeks after surgery.

Materials and Methods

In this prospective study, all patients qualified for the study were operated on in the Department and Clinic of Laryngology of the Medical University of Silesia in Katowice in the years 2021-2023, due to chronic bilateral sinusitis, confirmed by computer tomography of the sinuses (inclusion criteria). The diagnosis was made in accordance with the currently applicable EPOS 2020 guidelines.

A total of 180 patients were enrolled for the study (92 men and 88 women, average age 51.9 years). All patients who qualified for surgical treatment were operated on with the use of FESS for the first time on both sides, they did not suffer from hypertension or required surgical correction of the nasal septum (both were exclusion criteria). After the surgical procedure, one of the 3 types of above-mentioned commercially available dressings was applied in one side of the nasal cavity, while on the other side, a tamponade with a seton soaked with antibiotic and steroid ointment (due to its anti-inflammatory properties) in a rubber finger made of latex was used. A total of 180 patients after signing an informed consent were enrolled in the study, which means that a total of 360 intranasal dressings were applied (2 dressings in each patient, for both nasal cavities). After the surgical procedure, 4 different types of intranasal dressings were used in the randomized patients, as referred to above. Thus, a total of 60 NasalSponger® dressings, 60 MerocelPope® and 60 RapidRhino® dressings were used for the study, along with 180 tamponades in latex finger. In this way, 4 data groups were distinguished, depending on the type of dressing used after endoscopic surgery. All dressings were removed on the second day after surgery.

The approval of the Bioethical Commission of the Medical University of Silesia in Katowice, No. KNW/0022/KB289/18, was provided to conduct the research.

Characteristics of biomaterials used in dressings

NasalSponge® (MDD Medical Devices) is a haemostatic nasal sponge, sterile, absorbent, meant for single use, composed of PVA (polyvinyl alcohol) expanding sponge with a haemostatic gauze cover with a string attached, which simplifies the removal of the dressing (FIG. 1). Following the contact with fluid/water, the gauze cover can form a viscous gel and quickly stop capillary bleeding. In the meantime, the expanding sponge provides controlled pressure at the bleeding site. At the same time, the expanding sponge provides the possibility to control the pressure exerted on the bleeding site. The double function allows to achieve haemostasis easily. The dressing adapts to the anatomical shape of the nasal cavity. It does not stick to the tissue, thereby reducing possible complications such as clots or bleeding. NasalSponge has a double haemostatic function, which allows to: absorb body fluids and form gel through the outer layer of haemostatic gauze and allows blood coagulation, in order to accelerate physiological haemostasis (during contact of the gel with the wound surface). The outer part of the tampon, which is made of haemostatic gauze, turns into a gel after contact with blood; the mechanism of blood coagulation is activated to accelerate physiological haemostasis. The inner part of the tampon, made of a self-expanding sponge, can be expanded to exert adequate compression on the surface of the wound and elicit physical haemostasis by compression. The gel structure of the haemostatic gauze provides a moisture-containing environment to accelerate the epithelialization process of the nasal mucosa, it reduces damage and the possibility of re-occurrence of bleeding. The benefits of using this type of intranasal dressing comprise the safety of use, absence of side effects, rapid haemostasis, provision of a moist environment adjacent to the wound environment, and acceleration of the healing process, as well as no tampon sticking to the wound, lower risk of secondary trauma, ease of use, and painless application and removal of the tampon. The manufacturer recommends using the product for 24-48 hours and for a maximum of 72 hours if no active bleeding occurs. These tampons do not possess antibacterial properties. Before removing the sponge from the nose, one should instill saline solution into the nasal cavity and several minutes later gently remove the product. A total of 60 such dressings were applied.

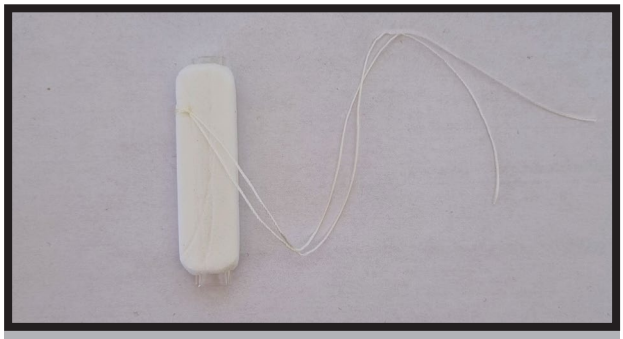

FIG. 1. NasalSponge type of dressing with string.

The second material examined was MerocelPope® (MP) dressing consisting of a microporous Merocel sponge made from high-density vinyl alcohol polymer (PVA) with oxidized cellulose (FIG. 2). This material maximizes the absorption and impermeability of tampons and minimizes pain and bleeding when tampons are removed. Fast-expanding tampons stop bleeding via gentle and even application of pressure upon the tissues, with platelets accumulating on the surface, which accelerates the formation of clots. 60 such dressings were applied.

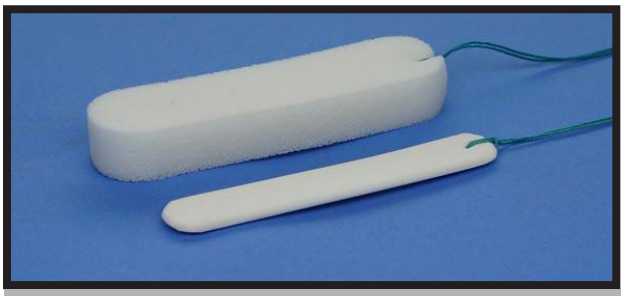

FIG. 2. MerocelPope type of dressing.

The third dressing that was examined was RapidRhino® made on the basis of carboxymethylcellulose (CMC – CarboxyMethyloCellulose) – a derivative of cellulose, whose innovative nature consists in double action: traditional wound tamponage, as well as accelerated haemostasis (FIG. 3). RapidRhino dressings accelerate platelet aggregation (which causes faster wound healing), perfectly protect the wound (which prevents infections), and do not cause secondary bleeding during their removal. These dressings, after preliminary preparation by a doctor (soaking in sterile water), are covered with hydrocolloid gel, which significantly facilitates their application and removal from the nasal cavity. They are designed for various types of treatments such as septorhinoplasty, turbinectomy, polypectomy, and FESS. A total of 60 such dressings were applied.

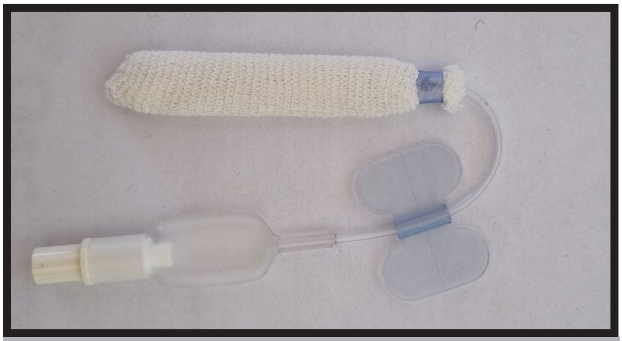

FIG. 3. RapidRhino type of dressing.

The fourth type of dressing applied was seton tamponade with antibiotic and steroid ointment in the latex glove finger (Routine nasal pack – RNP), commonly used in laryngology (FIG. 4). This type of dressing was applied in each surgically treated patient to one of the nasal passages, that is, a total of 180 of such dressings were applied (in each patient together with one of the three types of dressings mentioned above applied on the other side) (FIG. 5). It allowed us to compare modern commercial dressings with RNP in each patient.

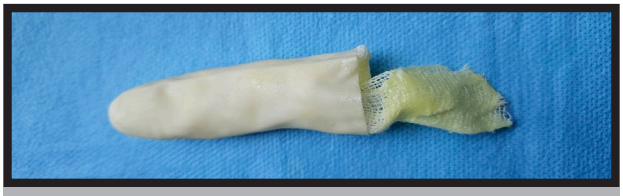

FIG. 4. Routine nasal pack – seton tamponade with antibiotic ointment (Oxycort) in latex surgical glove finger.

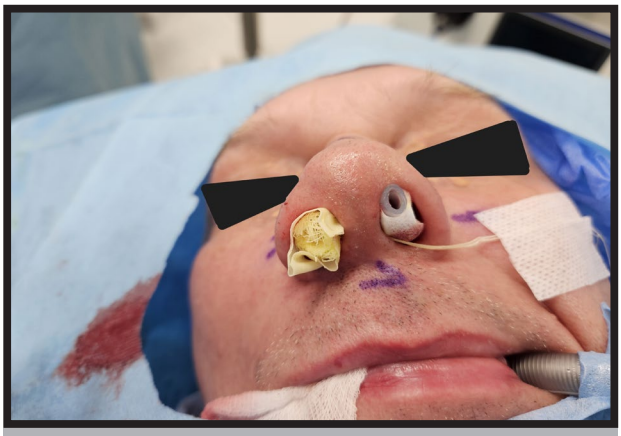

FIG. 5. Patient after surgery with bilateral intranasal dressings.

As mentioned above, four parameters were evaluated. The first parameter assessed was the haemostatic effectiveness of the dressing used. The assessment was carried out after the removal of the intranasal dressing on the second day after the surgery. The second evaluated parameter was the assessment of the level of pain in the nasal area during the application of the nasal dressing. In this case, the level of pain was subjectively assessed by the patient by means of visual analog scale (VAS) ranging from 0 and 10, the extremes being "absence of pain" – 0 points and "the most severe pain you can imagine" - 10 points. The third parameter evaluated was the assessment of pain experienced during dressing removal, also according to the VAS scale described above. The fourth parameter assessed was the development of postoperative adhesions within the nasal cavity. The presence of adhesions was always assessed by the surgeon performing the procedure during postoperative follow-up visits at weeks 4 and 8 after surgery. The study was conducted on both sides, using an endoscope with angles of 0° and 30°.

Statistical analysis

The results were subject to statistical analysis. At the beginning, descriptive statistics (percentage values) were calculated. The tests that were used to compare between the groups were: chi-squared test with Yates's correction ($\chi 2$) and Kruskal-Wallis test. The analysis was performed using STATISTICA 13.3 Tibco software. Statistical significance was assumed at the level of $p < 0.05$.

Results and Discussions

The results obtained are presented in the four above-mentioned ranges, i.e., the effectiveness of haemostatic action, assessment of the level of postoperative pain during dressing application, and assessment of pain experienced during dressing removal and assessment of the proneness for the formation of postoperative adhesions in the nasal cavity. The total number of subjects was 180 patients, which entails 360 intranasal dressings. Dressings of the following types: NasalSponge® (NS), MerocelPope® (MP), and RapidRhino® (RR) were applied in 60 patients each (60 nasal cavities), whereas seton with ointment in rubber glove finger (Routine nasal pack - RNP) was applied in 180 patients (180 nasal cavities).

Comparison of haemostatic properties of dressings

Bleeding after removal of the intranasal dressing of the NS type, which required re-establishment of tamponade, was found in 3 patients, after removal of the intranasal dressing of the MP type in 4 patients, in case of RR type of dressing, also in case of 3 patients, while in the case of 9 patients with RNP dressings the above was required (FIG. 6). Statistical analysis showed no differences between different types of dressings ($\chi 2 = 0{,}247$; $p = 0.967$).

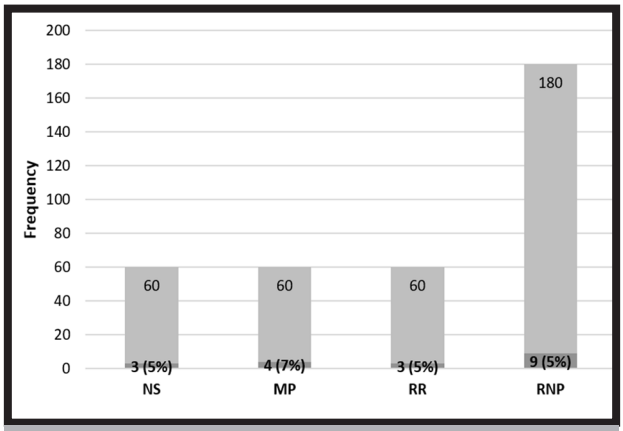

FIG. 6. Frequency of bleeding after removal of an intranasal dressing requiring tamponade. Explanation of abbreviations used: NasalSponge® (NS), MerocelPope® (MP), RapidRhino® (RR) (nasal cavities per each type of dressing, n = 60) and Routine nasal pack (RNP) (n = 180 nasal cavities).

Pain level after surgery

All patients qualified for the study assessed the level of postoperative pain on VAS scale. The pain assessment scores were between 0 and 6. In the NS-type dressing group, the average pain level was 3.2 (scores ranging from 2 to 5). For patients with MP dressings applied, the pain levels reported amounted to 3.1, on average (score range from 0 to 5). For patients with applied RR dressings, the pain levels reported amounted to 2.9, on average (score range from 0 to 5). For patients with applied RNP tamponage, the pain levels reported amounted to 3.1, on average (score range from 2 to 8). The difference in the level of postoperative pain associated with specific dressings between the different types of dressings was not statistically significant ($p = 0.399$) (FIG. 7).

The level of pain experienced when intranasal dressings were removed

All patients enrolled in the study indicated on the VAS scale the level of pain experienced when removing the intranasal dressing. The pain levels indicated ranged from 2 to 7.

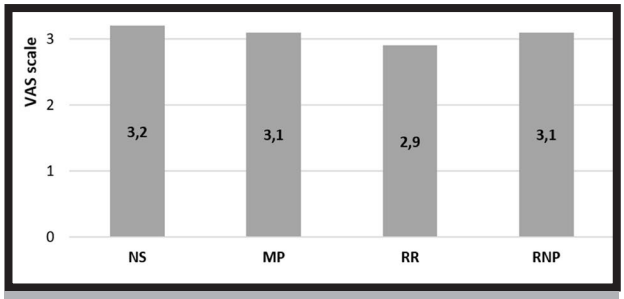

FIG. 7. Assessment of pain experienced during the removal of intranasal dressings 2 days after surgery) with the use of VAS scale. Explanation of abbreviations used: NasalSponge® (NS), MerocelPope® (MP), RapidRhino® (RR), Routine nasal pack (RNP).

In the case of dressings of NS type, the pain levels reported by patients amounted to 4.1, on average (range 3-7), in the case of dressings of MP type – 4.3 (range 2-7), in the case of dressings of RR type – 3.9 (range 3-7) while in the case of dressings of RNP type – 4.4 (range 3-7). No statistically significant differences were observed in the level of postoperative pain during the removal of internal dressing between the assessed types of dressings (p = 0.308) (FIG. 8).

Proneness to the formation of adhesions in middle nasal meatus

Endoscopic assessment of nasal cavities during follow-up visits 4 and 8 weeks after surgery revealed the development of unwanted nasal adhesions in 4 patients with dressings of NS type, 3 patients with dressings of MP type, 4 patients with dressings of RR type, and 9 patients with dressings of RNP type. No statistically significant differences were noted as regards the proneness to form adhesions, using the above-mentioned four types of dressings ($\chi 2 = 0{,}851$, p = 0.837) (FIG. 9).

Thanks to the use of intranasal dressings, we can control postoperative bleeding and the formation of adhesions in the middle nasal meatus, and can also minimize the level of pain associated with nasal tamponade. The results presented by us show that all types of dressings are effective in achieving postoperative haemostasis. Even in the case of significant intraoperative bleeding, these dressings are fully sufficient. Our study revealed that the use of the above 4 types of commercial dressings was associated with low levels of postoperative pain. The formation of adhesions within the middle nasal meatus after removal of ethmoidal cells, due to the tendency to lateralization of the central auricle, can significantly reduce the functional effect of surgery performed. In the world literature, the frequency of formation of unwanted adhesions is described in 1-35% of cases. An ideal postoperative dressing, in addition to good haemostatic properties, should also prevent the formation of adhesions. The results of our research showed that the percentage of adhesions after the use of all types of dressings applied by us was comparable (the differences were not statistically significant).

Haemostatic substances that are part of intranasal dressings have a double role to perform. Small sponge dressings covered with carboxymethylcellulose mesh can serve as a separator in the surgically treated region of the ethmoid sinuses, while larger ones are placed on the common nasal passages/meatuses and play mainly a haemostatic role. (RapidRhino® Nasal Dressing). On the other hand, removable tamponades made from oxidized cellulose in the form of sponges of different sizes perform haemostatic function mainly by compression (Merocel®).

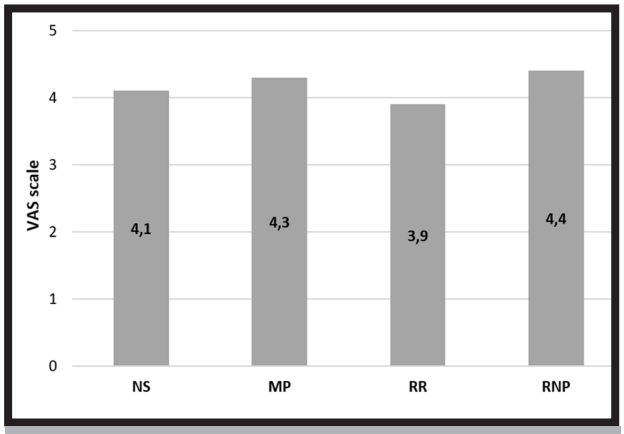

FIG. 8. Assessment of pain during the application of intranasal dressings (for 2 days after surgery) with the use of VAS scale. Explanation of abbreviations used: NasalSponge® (NS), MerocelPope® (MP), RapidRhino® (RR) (n = 60 nasal cavities per each type of dressing) and Routine nasal pack (RNP) (n = 180 nasal cavities).

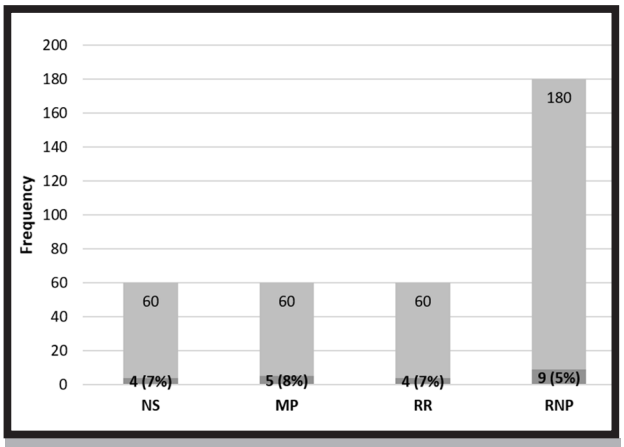

FIG. 9. Assessment of proneness to the formation of adhesions in nasal cavity, 4 and 8 weeks after the surgery. Explanation of abbreviations used: NasalSponge® (NS), MerocelPope® (MP), RapidRhino® (RR) (n = 60 nasal cavities per each type of dressing), and Routine nasal pack (RNP) n = 180 nasal cavities).

Conclusions

The application of intranasal dressings: NasalSponge®, MerocelPope®, RapidRhino® and Routine nasal pack is associated with a low level of pain both during the functioning of the dressing in the nasal cavity and in the course of removal of the dressing, a good haemostatic effect, and good effectiveness in preventing the formation of postoperative adhesions within the nasal cavity.

No statistically significant differences were demonstrated for the 4 intranasal types of dressings assessed as regards the haemostatic effect, the level of pain experienced when the dressing was in place in the nasal cavities, and during the removal of the dressing, assessed on the VAS scale, as well as concerning the formation of intra-nasal adhesions.

The level of pain assessed subjectively by the patient by means of Visual Analog Scale (VAS), after surgery and during the removal of the intranasal dressing did not differ statistically significantly.

No statistically significant differences were found in the frequency of formation of postoperative adhesions in the nasal cavity after the use of each of the 4 types of intranasal dressings assessed, provided that dressings were carefully applied/placed between the central auricle and the lateral nasal wall.

In conclusion, none of the analyzed 4 types of intranasal dressings proved to be distinctly advantageous. Their properties are comparable within the range of evaluated parameters. The obtained results do not indicate significant differences between the four types of dressings.

Acknowledgements

The study was conducted using the financial resources of the Statutory Research of the Medical University of Silesia in Katowice No. PCN-1-197/N/1/K.

ORCID iD

A. Maou: https://orcid.org/0009-0004-2865-9816
W. Likus: https://orcid.org/0000-0002-4738-6102
A. Długosz-Karbowska: https://orcid.org/0000-0002-3067-1935
J. Pilch: https://orcid.org/0000-0002-2682-4708
J. Markowski: https://orcid.org/0000-0003-3416-7354

References

[1] Fokkens W.J., Lund V.J., Hopkins C., et al.: European Position paper on rhinosinusitis and nasal polyps EPOS 2020, Rhinology 58(29) (2020).
[2] Côté D.W., Wright E.D.: Triamcinolone-impregnated nasal dressing following endoscopic sinus surgery: a randomized, double-blind, placebo-controlledstudy. Laryngoscope 120(6) (2010) 1269-1273.
[3] Verim A., Seneldir L., Naiboğlu B., Karaca Ç.T., Külekçi S., et al.: Role of nasal packing in surgical outcome for chronic rhinosinusitis-with polyposis. Laryngoscope 124(7) (2014) 1529-1535.
[4] Burduk P.K., Wierzchowska M., Grześkowiak B., et al.: Clinical outcome and patient satisfaction using biodegradable (NasoPore) and non-biodegradable packing, a double-blind, prospective, randomized study. Braz J Otorhinolaryngol 83(1) (2017) 23-28.
[5] Wormald P.J., Boustred R.N., et al.: A prospective single-blind randomized controlled study of use of hyaluronic acid nasal packs in patients after endoscopic sinus surgery. Am J Rhinol. 20(1) (2006) 7-10.
[6] Szczygielski K., Rapiejko P., Wojdas A., Jurkiewicz D.: Use of CMC foam sinus dressing in FESS. Eur Arch Otorhinolaryngol. 267(4) (2010) 537-540.
[7] Catalano P.J., Payne S., Thong M.: Clinical evaluation of a fully synthetic middle meatal stent for safety and tolerability. Otolaryngol Head Neck Surg. 144(3) (2011) 452-456.
[8] Chandra R., Kern R.: Advantages and disadvantages of topical packing in endoscopic sinus surgery. Curr. Opin. Otolaryngol. Head Neck Surg. 12 (2204) 21-26.
[9] Orlandi R., Lanza D.: Is nasal packing necessary following endoscopic sinus surgery? Laryngoscope 114 (2004) 1541-1544.
[10] Jurkiewicz D., Rogowski M., et al.: Evaluation of fully biodegradable nasal packings in functional endoscopic sinus surgery – a multicentre study. Polish Journal of Otolaryngology 69(1) (2015) 11-16.
[11] Zhou J.C., Zhang J.J., Zhang W., et al.: Efficacy of chitosan dressing on endoscopic sinus surgery: a systematic review and meta-analysis. Eur Arch Otorhinolaryngol. 274(9) (2017) 3269-3274.
[12] Chen J., Wang X., et al.: Influence of hyaluronan nasal dressing on clinical outcome after endoscopic sinus surgery: A systematic review and meta-analysis. Am J Rhinol Allergy 31(4) (2017) 256-259.
[13] Liu R., Gong Z.: Effect of chitosan-based gel dressing on wound infection, synechia, and granulations after endoscopic sinus surgery of nasal polyps: A meta-analysis. Int Wound J. 19(8) (2022) 2146-2153.
[14] Szczygielski K., Rapiejko P., Wojdas A., Jurkiewicz D.: Use of CMC foam sinus dressing in FESS. Eur Arch Otorhinolaryngol. 267(4) (2010) 537-540.
[15] Grzeskowiak B., Wierzchowska M., Walorek R., et al.: Steroid vs. antibiotic impregnated absorbable nasal packing for wound healing after endoscopic sinus surgery: a randomized, double blind, placebo-controlled study. Braz J Otorhinolaryngol. 85(4) (2019) 473-480.
[16] Kumarasamy G., Ramli R.R., Singh H., Abdullah B.: Tualang honey versus steroid impregnated nasal dressing following endoscopic sinus surgery: a randomized controlled trial. J Complement Integr Med. 18(2) (2020) 433-438.
[17] Wierzchowska M., Kalińczak-Górna P., et al.: Bioabsorbable dressing impregnated with betamethasone and ciprofloxacin after endoscopic sinus surgery: A randomized, double-blind, placebo-controlled study. Ear Nose Throat J. (2021) 1455613211062457.
[18] Sow Y.L., Tang I.P., Kho J.P.Y., Prepageran N.: Pilot study comparing steroid-impregnated and non-steroid-impregnated absorbable nasal dressing following endoscopic sinus surgery. Med J Malaysia 73(4) (2018) 244-248.
[19] Kühnel T.S., Hosemann WG, Weber R.: Postoperative Versorgung bei Nasennebenhöhleneingriffen [Postoperative treatment following paranasal sinus surgery]. HNO 69(6) (2021) 517-528.
[20] Valentine R., Wormald P.J.: Nasal dressings after endoscopic sinus surgery: what and why? Curr Opin Otolaryngol Head Neck Surg. 18(1) (2010) 44-48.
[21] Adriaensen G.F., Lim K.H., Fokkens W.J.: Safety and efficacy of a bioabsorbable fluticasone propionate-eluting sinus dressing in postoperative management of endoscopic sinus surgery: a randomized clinical trial. Int Forum Allergy Rhinol. 7(8) (2017) 813-820.
[22] Hobson C.E., Choby G.W., Wang E.W., Morton S.C., Lee S.: Systematic review and metaanalysis of middle meatal packing after endoscopic sinus surgery. Am J Rhinol Allergy. 29(2) (2015) 135-140.
[23] Valentine R., Wormald P.J.: Are routine dissolvable nasal dressings necessary following endoscopic sinus surgery? Laryngoscope. 120(10) (2010) 1920-1921.
[24] Shen H., Xiao S.F, Li T.C., et al.:Clinical efficacy of rapid Rhino Stammberger sinus dressing following endoscopic sinus surger]. Zhonghua Er Bi Yan Hou Tou Jing Wai Ke Za Zhi. 43(10) (2008) 782-785.
[25] Piski Z., Gerlinger I., Nepp N., Revesz P., Burian A., et al.: Clinical benefits of polyurethane nasal packing in endoscopic sinus surgery. Eur Arch Otorhinolaryngol. 274(3) (2017) 1449-1454.
[26] Qu J., Ma J., Zhou B., Huang Q., et al.: Efficacy and safety of pulmicort repulas-impregnated nasal dressing following endoscopic sinus surgery: a randomized, single-blind, placebo-controlled study. J Clin Otorhinolaryngol Head Neck Surg, 34(6) (2020) 541-545.
[27] Dal T., Bahar S.: The clinical outcomes of using a new cross-linked hyaluronan gel in endoscopic frontal sinus surgery. Eur Arch Otorhinolaryngol. 274(9) (2017) 3397-3402.
[28] Samarei R., Rasouli J., Mehdikhani F.: Efficacy of triamcinolone acetonide-impregnated Gelfoam nasal pack in management of chronic sinusitis with nasal polyps following endoscopic sinus surgery: a perfectly matched, placebo-controlled trial study. Eur Arch Otorhinolaryngol. 279(6) (2022) 2915-2924.
[29] Kim S.L., Kim S.D., Na H.S., Kim J.W., et al.: The efficacy of cotton ball packing after endoscopic sinus surgery: A prospective, randomized, controlled trial. Auris Nasus Larynx. 46(5) (2019) 742-747.
[30] Huang Z., Zhou B.: Comparison of Absorbable Packing versus No Packing in Wound Healing after Endoscopic Sinus Surgery: A Systematic Review and Pooled Analysis. ORL J Otorhinolaryngol Relat. 83(6) (2021) 404-411.
[31] Zhang M., Ryan P.J., Shashinder S.: Efficacy of Absorbable Steroid-Impregnated Nasal Packing in Functional Endoscopic Sinus Surgery for Chronic Rhinosinusitis: A Systematic Review. Laryngoscope. 131(8) (2021) 1704-1714.
[32] Hong S.D., Kim J.H., Dhong H.J., Kim H.Y., et al.: Systemic effects and safety of triamcinolone-impregnated nasal packing after endoscopic sinus surgery: a randomized, double-blinded, placebo-controlled study. Am J Rhinol Allergy. 27(5) (2013) 407-410.
[33] Wang Y.P., Wang M.C., Chen Y.C., Leu Y.S., Lin H.C., Lee K.S.: The effects of Vaseline gauze strip, Merocel, and Nasopore on the formation of synechiae and excessive granulation tissue in the middle meatus and the incidence of major postoperative bleeding after endoscopic sinus surgery. J Chin Med Assoc. 74(1) (2011) 16-21.

LASER FUNCTIONALIZATION OF MEDICAL SILICONE SURFACE MICROSTRUCTURE AND INVESTIGATION OF ITS ANISOTROPIC TRIBOLOGICAL PROPERTIES

Adam Patalas[1*], Mariusz Winiecki[2*], Paweł Zawadzki[1], Ryszard Uklejewski[2]

[1] Institute of Mechanical Technology, Poznan University of Technology, Piotrowo 3, 60-965 Poznan, Poland
[2] Department of Constructional Materials and Biomaterials, Faculty of Materials Engineering, Kazimierz Wielki University, Jan Karol Chodkiewicz Street 30, 85-064 Bydgoszcz, Poland
*e-mail: adam.patalas@put.poznan.pl; winiecki@ukw.edu.pl

Abstract

In this study, the assessment of the possibility of imparting anisotropic tribological properties to medical silicone surfaces using laser surface texturing was performed. The transversal-shaped microgrooves were laser-textured on the surface of the silicone samples applying different angles of incidence of the laser beam (α) ranging from 0° to 40°. The surface characteristics of the laser-textured silicone surface were performed by optical microscopy, surface 3D topography measurements, and contact angle measurements; the tribological tests were carried out under technically dry friction conditions and friction with lubrication conditions. The results showed: a significant increase in surface texture parameters values with Sq values ranging from 7.57 μm for α = 0° to 36.9 μm for α = 10°, compared to the non-textured sample 1.52 μm, increased hydrophilicity of the textured surfaces for most samples demonstrated by contact angle measured values for α = 0° sample showing the largest contact angle 126° as compared to the non-textured samples 103°. The produced anisotropic microstructure of the textured silicone surface, i.e. its directionality, is evidenced by obtained values of the texture aspect ratio (Str) tending to 0.00 for all textured samples. Changes in the friction coefficient's directionality in the forward and backward directions were noted for α values above 20° for both dry conditions and friction with lubrication conditions. We can conclude that laser surface texturing allows for the effective functionalization of a medical silicone surface in terms of the anisotropy of its tribological properties.

Keywords: *silicone, laser surface texturing, laser surface functionalization, friction, anisotropic tribological properties*

Introduction

Silicones, also known as polysiloxanes, are organosilicon polymers that have found widespread and diverse applications for medical and implantable devices since the 1940s [1]. It is due to their superior biocompatibility with multiple components, compatibility with many sterilization methods, resistance to repeated sterilization and biodurability when interacting with host tissues [2,3]. In terms of physicochemical properties beneficial for their use in the medical field are silicones' excellent chemical inertness and thermostability, hydrophobicity, low surface energy, appropriate mechanical properties (modulus and stretchability) with durability and ease of moulding by many methods [4-6]. Silicones are versatile and can be formulated into various forms, such as silicone elastomer, silicone gel, or silicone adhesive, which determines their intended applications. Medical applications of silicones include, but are not limited to, contact lenses [7], breast implants [8], drains [9,10] and shunts [11], catheters [12], reconstructive gel fillers [13] and sheeting [14], cranio-maxillo-facial implants [15,16], scaffolds for nerve regeneration [17], and implants for small joint arthroplasty [18], as well as for devices with a non-silicone substrate that had been silicone-coated to provide less host reaction, such as needles, syringes, or blood collection vials.

The working surfaces of the material often require modification that gives them specific properties determined by the functions they are to perform. Surface functionalization allows for enhancing their performance for example in terms of hydrophilization by increasing their surface wettability [19,20], enhancing the tribological properties of the material, such as load capacity, wear resistance and coefficient of friction [21-24] or modifying the surface properties related to cell/surface interactions i.e., providing the surface topography endorsing tissue/materials integration through cells adhesion and activity [25-28]. The micro- and nanostructural functionalization of the work surface can be performed by many methods such as electric discharge texturing [29], focused ion beams [30], electrochemical machining [31], hot embossing [32], lithography, or mechanical texturing [33]. Laser surface texturing (LST) is a relatively new and widely explored method for acquiring specific physical surface properties desired in functional surfaces that allow surface structuring by producing a defined pattern or texture on a work surface with excellent controllability [34,35].

The aim of the work is to assess the possibility of imparting anisotropic tribological properties to medical silicone surfaces using laser surface texturing.

[Engineering of Biomaterials 171 (2023) 23-29]

doi:10.34821/eng.biomat.171.2023.23-29

Submitted: 2023-11-10, Accepted: 2023-12-11, Published: 2023-12-14

Materials and Methods

Sample surface modification

In this study, medical-grade RTV-2 silicone, approved for skin contact, and designated as SIL 25, was used. It is a two-part mixture for curing silicone at room temperature. Samples in the shape of rectangular prisms measuring 20x60 mm and 4 mm thick were moulded. After moulding, they were degassed using a vacuum pump, followed by curing at a temperature of 50°C for 45 min.

A blue laser (PLH3D-XT-10, Opt Lasers, Warsaw, Poland), with an output power of 0.5 W at 405 nm laser wavelength and square laser spot of 10 µm was used to produce transversal-shaped microgrooves on the surface of the sample. During the microgrooves texturing, the angle of incidence of the laser beam on the sample surface was varied while maintaining a constant power density of 8.8 kW/mm^2, which is approximately 80% of the maximum power density. The power density of the laser beam was selected experimentally, as it ensured the relatively highest repeatability of the texturing results. Depending on the set values angles of incidence of the laser beam on the sample surface of 0°, 10°, 20°, 30°, and 40°, the samples are referred to as LA0, LA10, LA20, LA30 and LA40, while the untextured sample is denoted as Raw. The scheme of geometry of laser-textured surface microgrooves is presented in FIG. 1.

Sample surface characterization

The surface morphology of the textured microgrooves was examined by applying an optical microscope and a 3D profilometry apparatus (PortableRL, Bruker Alicona, Raaba, Austria). The values of the geometric features of the microgrooves were determined. According to the microgrove geometry presented in FIG. 1, the following geometric features were measured: α – deviation of microgroove angle bisector from the normal to the sample surface (°), β – microgroove apex angle (°), d – microgroove depth (µm) and B – the distance between grooves (µm). The surface topography measurements were carried out by the focus-variation method combining an optical system's small depth of focus with vertical scanning to provide topographical and colour information from the focus variation. From the group 3D areal surface texture parameters described in [36,37] the parameters, such as the root mean square roughness (Sq), the maximum pit height (Sv), the texture aspect ratio (Str), skewness (Ssk) and kurtosis (Sku) were selected and measured with a cut-off wavelength of 800 µm. Moreover, the material ratio curves were determined and the valley void volume (Vvv) was evaluated. The accuracy of the measurements in terms of uncertainty was U = 50 nm.

Contact angle measurements on the laser-textured surface using the OCA 15Pro Goniometer (DataPhysics Instruments GmbH, Filderstadt, Germany) equipped with an automatic liquid drop dosing system. The dropping unit was set to the drop dosing volume of 2 µl and the drop dosing rate of 0.5 µl/s. Since Ringer's solution is a recognized SBF, it was used in this study in contact angle measurements [38]. The temperature in the laboratory room during the experiments was stable and amounted to 22.4°C. The static contact angle on a flat surface was calculated with dedicated goniometer software (SCA 20, DataPhysics Instruments GmbH, Filderstadt, Germany) by automatically detecting baselines and tangents. The accuracy of the contact angle measurement is considered ± 0.1°.

The tribological oscillating ball-on-flat tests were carried out using a Universal Mechanical Tester Tribometr (UMT TriboLab™, Billerica, Massachusetts, USA) according to the ASTM G133-22 standard [39]. The tribological tests were carried out under technically dry friction conditions and friction conditions with lubrication with the Ringer's solution, collagen hydrolyzate and silicone oil. The counter-sample as a stainless steel ball with a 10 mm diameter was applied. A surrounding climate chamber kept the environmental conditions constant at a temperature of 24°C ± 1°C and of 40% ± 1% relative humidity. The linear drive was used to apply a reciprocating movement of the velocity up to 10 mm/s, and a linear sliding length was set for 30 mm. The applied forces were controlled by sensors' module DFM-20 (UMT TriboLab™, Billerica, Massachusetts, USA) within the range of 0.2 N to 20 N and the contact force was set to 5 N ± 0.2 N.

Results and Discussion

The microscope images of the side views of textured samples are shown in FIG. 2. The measured values of geometric features of microgrooves laser-textured on a silicone material are provided in TABLE 1. Analyzing the obtained microscope images of the laser-textured microgrooves and their measured geometric features, it can be seen that the set laser beam angle is very close to the deviation of the microgroove angle bisector from the normal to the sample surface. The only significant difference is found for the LA10 sample. The largest groove depth was obtained for the LA10 sample and the smallest for LA0.

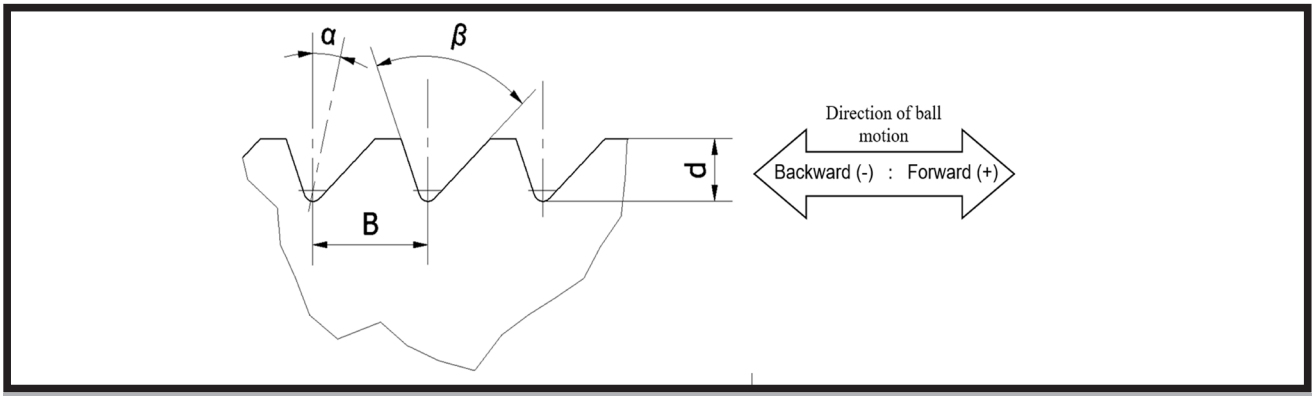

FIG. 1. Design of microgrooves geometry with annotated geometrical features: α – deviation of microgroove apex angle (briefly called also *'microgroove axis'*) bisector from the normal to sample surface (°), β – microgroove apex angle (°), d – microgroove depth (µm), B – distance between microgrooves (µm).

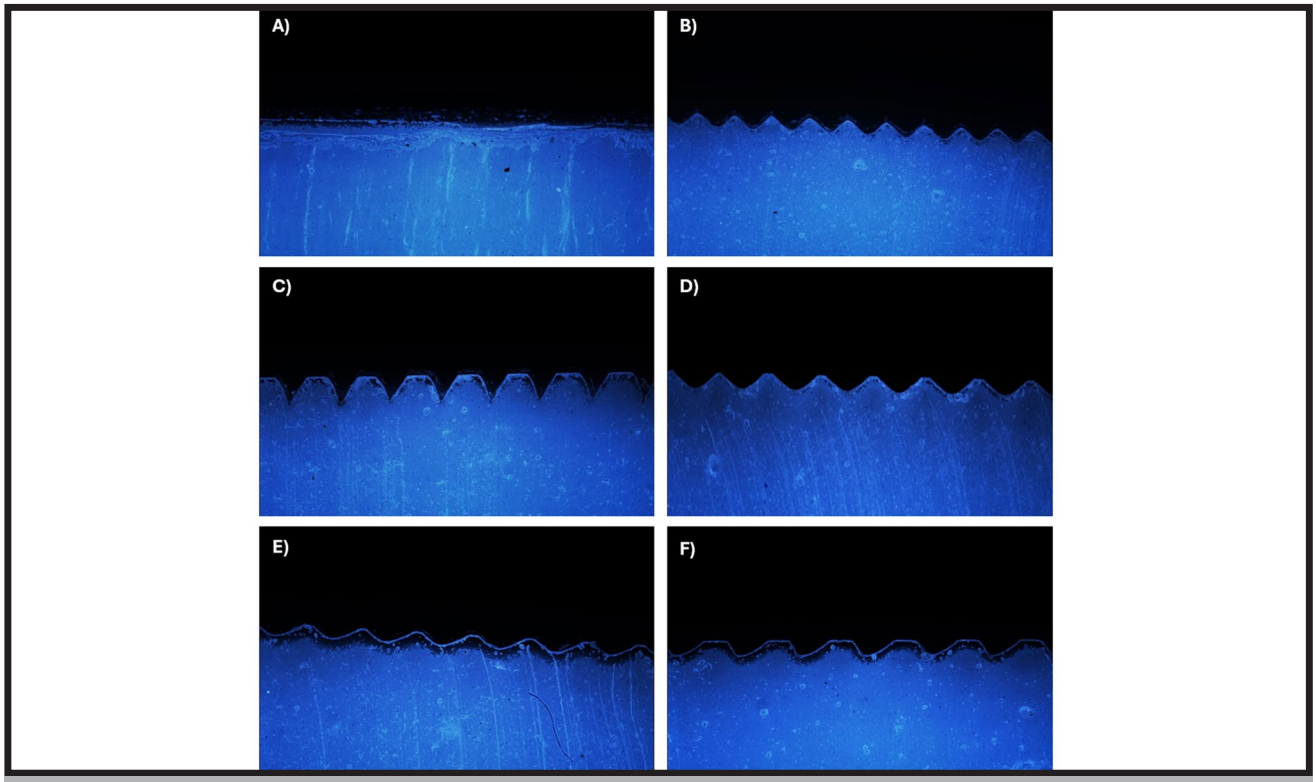

FIG. 2. Side views of laser-textured silicone material: A) Raw, B) LA0, C) LA10, D) LA20, E) LA30, and F) LA40.

TABLE 1. The values of geometric features of microgrooves laser-textured on a silicone material.

Sample	Set angle of laser beam (°)	α (°)	d (µm)	β (°)	B (µm)
LA0	0	0 ± 0	48 ± 4	34 ± 2	195 ± 10
LA10	10	14 ± 1	98 ± 3	41 ± 2	255 ± 8
LA20	20	18 ± 2	89 ± 4	57 ± 1	273 ± 8
LA30	30	30 ± 3	59 ± 4	51 ± 2	286 ± 9
LA40	40	41 ± 2	67 ± 1	59 ± 3	323 ± 9

FIGURE 3 shows the 2D surface topography of the microgrooves laser-textured on the silicone material surface. The material share curves created based on these representative areas are presented in FIG. 4. As it can be seen, a plateau was obtained for samples LA10-LA40. The sharpest groove notches were obtained for sample LA10. The groove notches of the remaining samples are characterized by a gentle valley/end.

In statistical terms, a significant increase in the Sq parameter values was observed due to surface texturization, as intended (TABLE 2). According to the assumptions, there was an increase in the maximum value for the valley's depth, as confirmed by the high values of the parameter Sv. From a tribological perspective, a notable feature is the change in the parameter Ssk value, which shifted from the baseline value of Ssk = -0.63 towards 0 for all surfaces. Consequently, there was an increase in the symmetry of the surface relative to the mean line, along with the kurtosis parameter Sku, which for textured surfaces takes values Sku ≤ 3, confirming the designed periodicity in the resulting surface layer structure. In terms of functional parameters, attention should be paid to Vvv, which increased several times for textured samples, potentially ensuring improvement in friction parameters, particularly in the presence of lubricants from a tribological standpoint. Following the assumptions, a significant directionality of the structure was achieved, which is confirmed by the values of the Str coefficient < 0.03.

The results of the contact angle measurement are presented in TABLE 3 and FIG. 5. The contact angle measurements revealed that the LA10 sample exhibited the largest contact angle. Interestingly, it was observed that the contact angle values for the LA10-40 samples consistently exceeded those of the untextured reference sample. It was not possible to correctly measure the contact angle for the LA0 sample, but as can be seen in FIG. 5A, the droplet spread in the microgrooves. This may be because the measuring liquid – Ringer's liquid, has a viscosity similar to water and did not form a stable drop. The measured one-second contact angle value for LA0 is 86.0 ± 4.9. This disparity in contact angle values between the LA0 sample and the other textured samples may be attributed to the presence of sharp-edged microgrooves in the former, facilitating enhanced drop penetration into the grooves. Conversely, in the textured samples (LA10-40), the limited liquid penetration into the valley spaces is anticipated, largely due to surface tension effects. FIGURE 5 presents the results of measuring the friction coefficient values for different environmental conditions. TABLE 4 presents the percentage increase of the directional coefficient of friction for different samples under various types of lubrication.

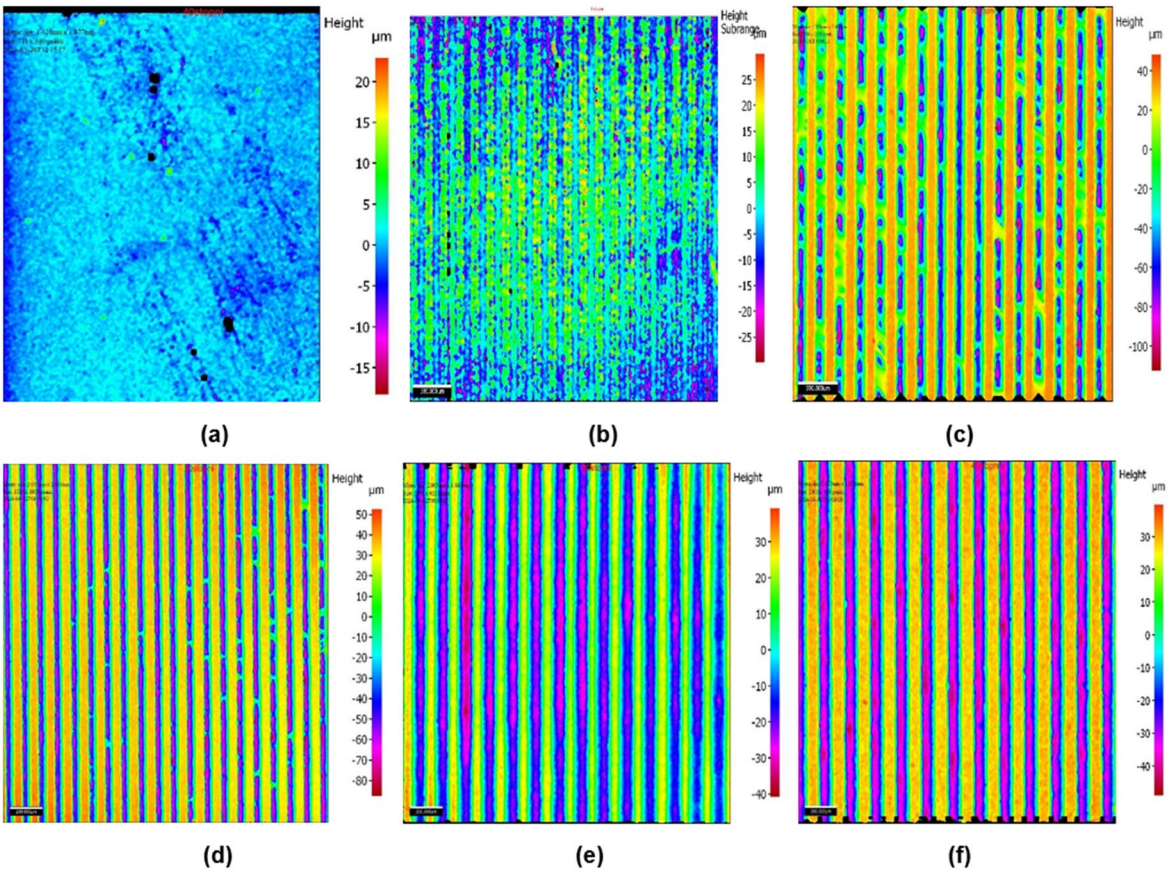

FIG. 3. 2D surface topography of the laser-textured silicone surface samples (left to right): Raw, LA0, LA10 (a-c), and LA20, LA30, LA40 (d-f).

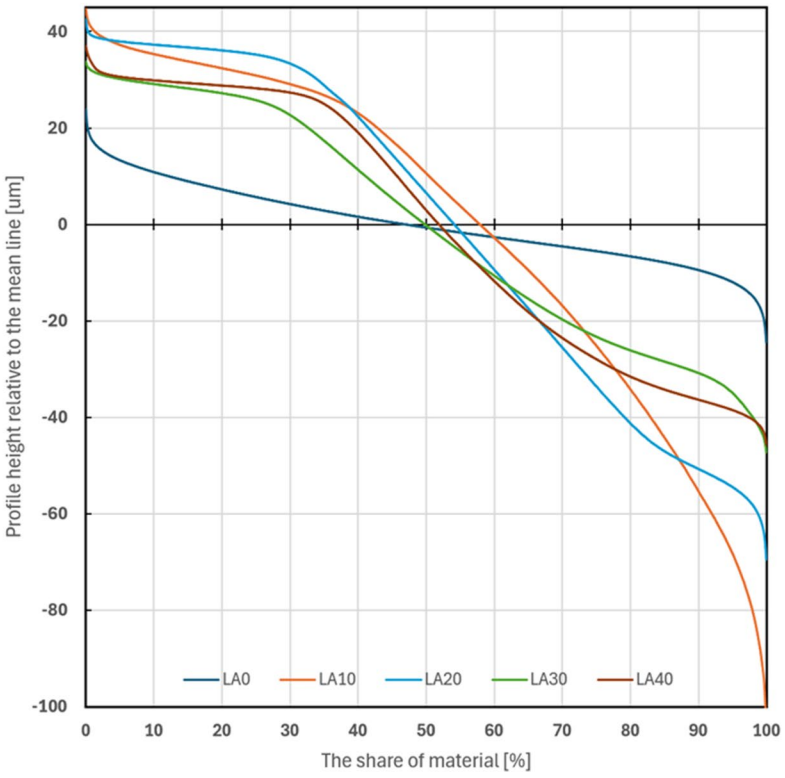

FIG. 4. Material share curves for representative areas of laser-textured silicone surface.

TABLE 2. The surface geometric parameters of the laser-textured silicone surface.

Sample	Raw	LA0	LA10	LA20	LA30	LA40
Sq	1.52	7.57	36.9	33.6	17.6	25.4
Sv	18.3	48.32	92.1	113.6	40.3	52.9
Str	0.38	0.04	0.03	0.03	0.04	0.04
Ssk	-0.63	0.055	-0.49	-0.225	0.204	-0.267
Sku	9.955	3	1.79	1.558	1.7	1.409
Vvv	0.254	1.043	3.06	1.722	0.921	1.052

TABLE 3. Average values of the surface contact angle.

Sample	Raw	LA0	LA10	LA20	LA30	LA40
Contact angle	103 ± 2	86 ± 5*	126 ± 3	124 ± 5	109 ± 3	118 ± 4

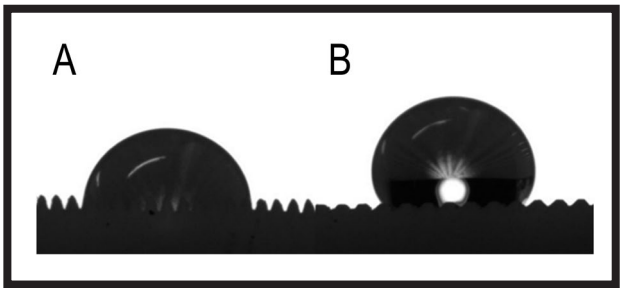

FIG. 5. Example contact angle measurement results: A) LA0, B) LA10.

From the data in FIG. 6, it can be seen that the average friction coefficients range from 0.13 to 1.30. The lowest measured values of the friction coefficient were measured for the combination under silicone oil lubrication conditions. For all measurements, the friction coefficient in the forward direction was lower than in the backward direction. The highest friction coefficient values were for: dry friction – sample LA10, friction in Ringer's fluid – sample LA30, friction in collagen hydrolyzate – sample LA30, friction in silicone oil – sample LA20. For samples tested in a dry environment, it is visible that the largest changes in the friction coefficient value are for samples LA20, LA30, and LA40. For samples tested in the Ringer's fluid and collagen hydrolysate environment, such a significant change was observed only for LA30 and LA40 samples. However, during tests in a silicone oil environment, the largest difference in directional friction coefficient values was observed for samples LA10 and LA20, while for LA10 sample this increase was the largest among all the measurements carried out and it was by 277%; the observed differences in directional friction coefficient values for applied lubricants may be related to different properties of water-based lubricants (Ringer's fluid, collagen hydrolyzate) and non-water-based lubricant (silicone oil).

TABLE 4. Percentage difference of directional coefficient of friction values in forward and backward directions.

Set angle Sample	Lubrication type and percentage increase of directional coefficient of friction			
	Dry	Ringer's fluid	Collagen hydrolyzate	Silicone oil
LA0	27%	11%	76%	22%
LA10	7%	5%	9%	277%
LA 20	114%	13%	7%	176%
LA 30	73%	64%	46%	38%
LA 40	77%	78%	39%	88%

FIGURE 7 compares friction coefficient values as a function of the linear position of the ball counter sample on the tested sample for the LA40 sample and the Raw sample in an oil-lubricated environment. As it can be observed, despite the presence of a lubricating environment (oil), the surface texturization leads to an increase in the friction coefficient values. However, in terms of the directional effect of the textured microstructure, a relatively constant difference between the coefficient of friction value in the forward direction (+) and backward direction (-) is evident.

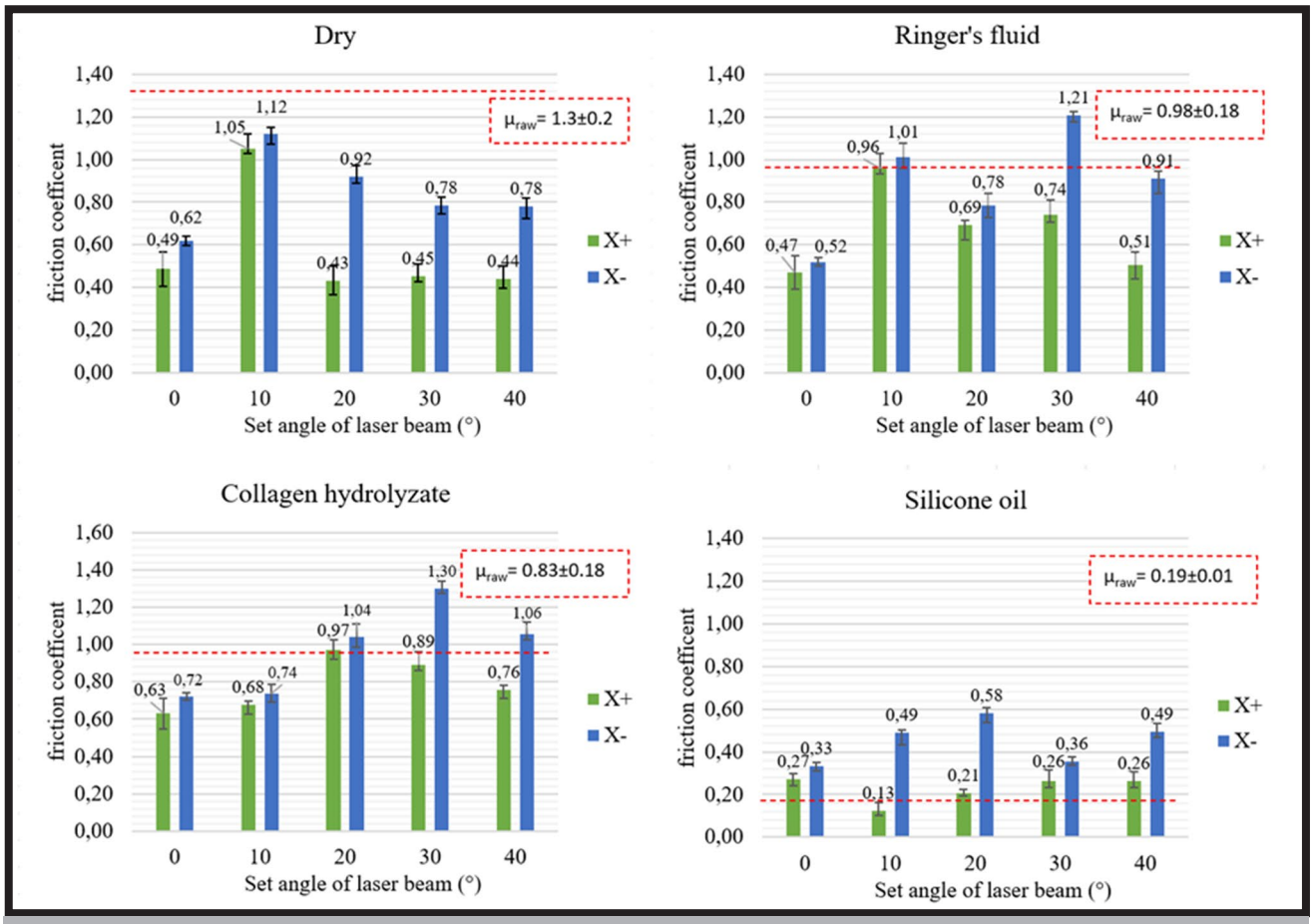

FIG. 6. Results of measuring the directional coefficient of friction values for 4 environmental conditions. Results for unmodified samples are presented as red dashed lines.

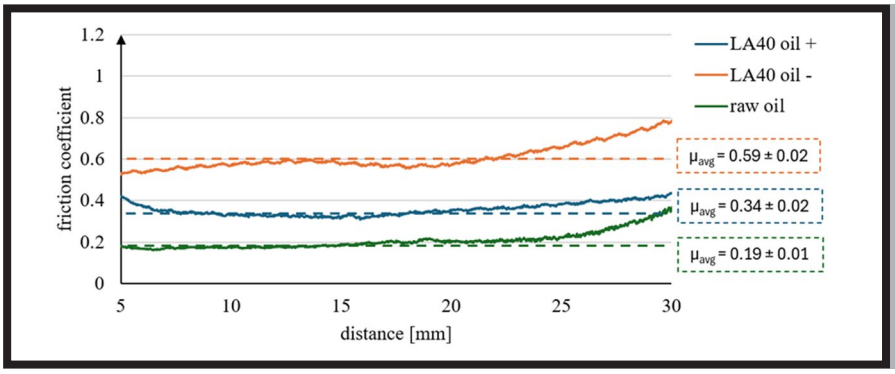

FIG. 7. Comparison of the directional coefficient of friction values as a function of the linear position of the ball counter sample on the tested sample for raw and LA40 textured surfaces in an oil-lubricated environment.

Conclusions and research perspectives

The performed laser texturing of medical silicone surface assures high accuracy of repeatability of surface texture parameters across the textured surface. Produced anisotropic microstructure of the textured silicone surface, i.e. its directionality, is evidenced by the measured values of the texture aspect ratio (Str) tending to 0.00 for all textured samples. The percentage differences in the directional coefficient of friction values registered in forward and backward directions for the laser beam angle setting values above 20° imparts the clearly evident directional anisotropy of the tribological properties of the textured surface.

So, we can conclude that laser surface texturing allows for effective functionalization of medical silicone surface in terms of its directional anisotropy of tribological properties.

Looking forward, future research directions should focus, in our opinion, on exploring the applicability of laser texturing to medical devices with rotationally symmetric elements. Such endeavours hold promise for optimizing the tribological properties of medical devices, thereby enhancing their performance and biocompatibility in clinical settings.

Acknowledgements

This research was funded by the Polish Ministry of Science and Higher Education as a part of an annual subsidy – project numbers: 0614/SBAD/1586.

ORCID iD

A. Patalas: https://orcid.org/0000-0001-5476-6739
M. Winiecki: https://orcid.org/0000-0002-3568-2473
P. Zawadzki: https://orcid.org/0000-0001-8153-8774
R. Uklejewski: https://orcid.org/0000-0002-3587-714X

References

[1] Allen L.V. Jr.: Compounding with Silicones. International Journal of Pharmaceutical Compounding 19(3) (2015) 223-230.
[2] Colas A.R., Curtis J.: Silicone Biomaterials: History and Chemistry & Medical Applications of Silicones. In: Ratner B.D., Hoffman A.S., Schoen F.J., Lemons J.E., Eds): Biomaterials Science: An Introduction to Materials in Medicine. Academic Press; 3rd edition, 2013. 82-91.
[3] Bračič M., Strnad S., Fras Zemljič L.: Silicone in Medical Applications. In: Bioactive Functionalisation of Silicones with Polysaccharides. SpringerBriefs in Molecular Science. Springer, Cham. 2018.
[4] Owen M.J.: Silicone Surface Fundamentals. Macromolecular Rapid Communications 42(5) (2021) e2000360.
[5] Marmo A.C., Grunlan M.A.: Biomedical Silicones: Leveraging Additive Strategies to Propel Modern Utility. ACS Macro Letters 12(2) (2023) 172-182.
[6] Zare M., Ghomi E.R., Venkatraman P.D., Ramakrishna S.: Silicone-based biomaterials for biomedical applications: antimicrobial strategies and 3D printing technologies. Journal of Applied Polymer Science 138(38) (2021) e50969.
[7] Ishihara K., Shi X., Fukazawa K., Yamaoka T., Yao G., Wu J.Y.: Biomimetic-Engineered Silicone Hydrogel Contact Lens Materials. ACS Applied Bio Materials 6(9) (2023) 3600-3616.
[8] Chao A.H., Garza R. 3rd, Povoski S.P.: A review of the use of silicone implants in breast surgery. Expert Review of Medical Devices 13(2) (2016) 143-156.
[9] Bakoš M., Kuťka M.: Drainage in Abdominal Surgery. Biomedical Journal of Scientific & Technical Research 2022 43(3) BJSTR. MS.ID.006912.
[10] Makama J.G., Ameh E.A.: Surgical drains: what the resident needs to know. Nigerian Journal of Medicine 17(3) (2008) 244-250.
[11] Srinivas D., Tyagi G., Singh G.J.: Shunt Implants - Past, Present and Future. Neurology India 69(Supplement) (2021) S463-S470.
[12] Lawrence E.L., Turner I.G.: Materials for urinary catheters: a review of their history and development in the UK. Medical Engineering & Physics 27(6) (2005) 443-453.
[13] Spiera R.F., Gibofsky A., Spiera H.: Silicone gel filled breast implants and connective tissue disease: an overview. Journal of Rheumatology 21(2) (1994) 239-245.
[14] Tian F., Jiang Q., Chen J., Liu Z.: Silicone gel sheeting for treating keloid scars. Cochrane Database of Systematic Reviews 1(1) (2023) CD013878.
[15] Ariani N., Visser A., van Oort R.P., Kusdhany L., Rahardjo T.B., Krom B.P., van der Mei H.C., Vissink A.: Current state of craniofacial prosthetic rehabilitation. International Journal of Prosthodontics 6(1) (2013) 57-67.
[16] Kumar A., Seenivasan M.K., Inbarajan A.: A Literature Review on Biofilm Formation on Silicone and Poymethyl Methacrylate Used for Maxillofacial Prostheses. Cureus 13(11) (2021) e20029.
[17] Yi S., Xu L., Gu X.: Scaffolds for peripheral nerve repair and reconstruction. Experimental Neurology 319 (2019) 112761.
[18] Moran S.L., Rizzo M.: Managing Difficult Problems in Small Joint Arthroplasty: Challenges, Complications, and Revisions. Hand Clinics 39(3) (2023) 307-320.
[19] Pereira R.S., Moura C.G., Henriques B., Chevalier J., Silva F.S., Fredel M.C.: Influence of laser texturing on surface features, mechanical properties and low-temperature degradation behavior of 3Y-TZP. Ceramics International 46 (2020) 3502-3512.
[20] Yu Z., Yang G., Zhang W., Hu J.: Investigating the effect of picosecond laser texturing on microstructure and biofunctionalization of titanium alloy. Journal of Materials Processing Technology 255 (2018) 129-136.
[21] Mao B., Arpith Siddaiah Y.L., Pradeep L.M.: Laser surface texturing and related techniques for enhancing tribological performance of engineering materials: A review. Journal of Manufacturing Processes 53 (2020) 153-173.
[22] Wang C., Li Z., Zhao H., Zhang G., Ren T., Zhang Y.: Enhanced anticorrosion and antiwear properties of Ti-6Al-4V alloys with laser texture and graphene oxide coatings. Tribology International 152 (2020) 106475.
[23] Wu Z., Bao H., Xing Y., Liu L.: Tribological characteristics and advanced processing methods of textured surfaces: A review. International Journal of Advanced Manufacturing Technology 114 (2021) 1241-1277.
[24] Bonse J., Kirner S.V., Griepentrog M., Spaltmann D., Krüger J.: Femtosecond Laser Texturing of Surfaces for Tribological Applications. Materials 11(5) (2018) 801.
[25] Tiainen L., Abreu P., Buciumeanu M., Silva F., Gasik M., Guerrero R.S., Carvalho O.: Novel laser surface texturing for improved primary stability of titanium implants. Journal of the Mechanical Behavior of Biomedical Materials 98 (2019) 26-39.
[26] Shukla P., Waugh D.G., Lawrence J., Vilar R.: Laser surface structuring of ceramics, metals and polymers for biomedical applications: A review. In Laser Surface Modification of Biomaterials; Woodhead Publishing: Cambridge, UK, 2016; pp. 281-299.
[27] Cunha W., Carvalho O., Henriques B., Silva F.S., Özcan M., Souza J.C.M.: Surface modification of zirconia dental implants by laser texturing. Lasers in Medical Science 37(1) (2022) 77-93.
[28] Han J., Zhang F., Van Meerbeek B., Vleugels J., Braem A., Castagne S.: Laser surface texturing of zirconia-based ceramics for dental applications: A review. Materials Science & Engineering C: Materials for Biological Applications 123 (2021) 112034.
[29] Jithin S., Joshi S.S.: Surface topography generation and simulation in electrical discharge texturing: A review. Journal of Materials Processing Technology 298 (2021) 117297.
[30] Kawasegi N., Ozaki K., Morita N., Nishimura K., Yamaguchi M.: Development and machining performance of a textured diamond cutting tool fabricated with a focused ion beam and heat treatment. Precision Engineering 47 (2017) 311-320.
[31] Patel D.S., Jain V.K., Shrivastava A., Ramkumar J.: Electrochemical micro texturing on flat and curved surfaces: simulation and experiments. International Journal of Advanced Manufacturing Technology 100 (2019) 1269-1286.
[32] Pettersson U., Jacobson S.: Tribological texturing of steel surfaces with a novel diamond embossing tool technique. Tribology International 39(7) (2006) 695-700.
[33] Costa H., Hutchings I.: Some innovative surface texturing techniques for tribological purposes. Proceedings of the Institution of Mechanical Engineers, Part J: Journal of Engineering Tribology. 229(4) (2015) 429-448.
[34] Shivakoti I., Kibria G., Cep R., Pradhan B.B., Sharma A.: Laser Surface Texturing for Biomedical Applications: A Review. Coatings 11 (2021) 124.
[35] Moskal D., Martan J., Honner M.: Scanning Strategies in Laser Surface Texturing: A Review. Micromachines 14 (2023) 1241.
[36] Stout K.J., Sullivan P.J., Dong W.P., Mainsah E., Lou N., Mathia T., Zahouani H.: The Development of Methods for The Characterisation of Roughness in Three Dimensions, Report EUR 15178 EN, European Commission, Brussels, 1993, ISBN 0-7044-1313-2
[37] ISO 25178-2:2021. Geometrical product specifications (GPS) — Surface texture: Areal — Part 2: Terms, definitions and surface texture parameters.
[38] Agathopoulos S., Nikolopoulos P.: Wettability and interfacial interactions in bioceramic-body-liquid systems. J Biomed Mater Res. Apr;29(4):421-9 (1995). doi: 10.1002/jbm.820290402.
[39] ASTM G133-22. Standard Test Method for Linearly Reciprocating Ball-on-Flat Sliding Wear.